

New experiments to probe the role of fractures in bedrock on river erosion rate and processes

Marion Fournereau¹, Laure Guerit¹, Philippe Steer¹, Jean-Jacques Kermarrec¹, Paul Leroy², Christophe Lanos³, H el ene Hivert⁴, Claire Astri e¹, Dimitri Lague^{1,2}

5 ¹Univ Rennes, CNRS, ~~G eosciences~~Geosciences Rennes, UMR 6118, 35000, Rennes, France

²Univ Rennes, CNRS, Lidar Platform, OSERen, UAR3343, Rennes, France

³Univ Rennes, Laboratoire de G enie Civil et G enie M ecanique, Rennes, France

⁴Univ Rennes, Inria, G eosciences Rennes - UMR 6118, IRMAR - UMR 6625, F-35000 Rennes, France

Correspondence to: Marion Fournereau (marion.fournereau@univ-rennes.fr) and Laure Guerit (laure.guerit@univ-rennes.fr)

10

Abstract

River erosion ~~via abrasion and plucking~~ is a fundamental process that impacts, among others, mountain landscape evolution. Mountain rock lithologies often exhibit bedding, joints, and fractures that are thought to alter the incision efficiency of rivers compared to intact, massive rocks. The presence of close enough planar mechanical discontinuities allows the creation and
15 entrainment of large blocks through plucking, a process that adds to abrasion, and potentially macroabrasion, by the transported
~~sediment transport, and incision at the base of hillslopes. It results from complex interactions between climate, tectonics, topography and the erodibility. Despite preliminary attempts to include shallow fracturing in theoretical models of bedrock. Despite its significant~~ incision and a couple of studies that quantified in situ the relative importance of abrasion and plucking
20 processes, we are still lacking ways to systematically probe the role, of fractures on bedrock erodibility remains poorly
~~understood as it is thought to aggregate several parameters. Among these, fractures in bedrock are assumed to exert a strong control over~~ erosion and thus, on landscape evolution. Systematic studies comparing fracture geometry and density rates and
bedrock river erosion are needed.
processes. Due to the complex interactions at play, we investigate this question via an experimental approach. ~~We develop an,~~
25 using a new erosion mill apparatus designed to erode a fractured concrete disk with a diameter of 17 cm. We simulate fractures
by embedding a 3D-printed plastic mesh in the concrete, using BVOH—a plastic that softens in cold water—creating
mechanical heterogeneities/weaknesses with a controlled pattern. We explore 10 different geometries and run 4 additional
experiments without fractures for control. We record the topographic evolution every 2 minutes by photogrammetry and derive
erosion maps by measuring elevation changes between successive scans. ~~Our results show that while fractures influence the~~
30 relative contributions of abrasion and plucking, no clear relationship emerges between average erosion rates and fracture
~~density or dip angle. However, we observe that the occurrence of plucking is related to the density and the dip angles of~~ fractures, and is favoured by intermediate density that scales with the size of the impactors, and intermediate dip angle that
ease the removal of blocks. We suggest that the main impact of plucking in our experiments is to change the location of erosion,
increasing the eroded surface area rather than accelerating overall erosion rates. However, but as plucking accounts for at most
one third of the total erosion of our disks, its occurrence does not significantly affect average erosion rates. These findings
35 emphasize the role of fractures on erosion mode and location, rather than on erosion rates. As erosion by plucking tends to
increase bed roughness compared to simple abrasion, this suggests that the fracture network can influence the flow field in
fractured bedrock rivers. This highlights the need to further explore the impact of fractures on riverbed erosion. Our results
show that fractures influence the morphodynamical evolution of the disks and the relative contributions of abrasion and
plucking. However, abrasion systematically remains the dominant erosion mechanism, with plucking contributing at most to
40 29 % of the total erosion for vertical fractures spaced by 20x20 mm², 40 % for one specific dip angle (67 °), and less than 10
% for most experiments. Average erosion rates show a modest (20 %) increase with the fraction of plucking, but do not show
a clear relationship with fracture density and the presence of fracture. We suggest that the rate of erosion by plucking is limited

by the depth and slow rate of horizontal fracture propagation between pre-existing vertical fractures, such that in our experimental setup, abrasion is systematically a dominant component. These findings emphasize the critical role of block preparation and loosening for plucking to be an effective process compared to abrasion. This new setup allows abrasion, macroabrasion, and plucking driven by bedload impacts to be studied in controlled situations, albeit with the well-known limits of abrasion mills and without the variety of natural processes that can drive fracture propagation. Further experiments should expand the parameter space of the erosion efficiency problem (i.e., sediment mass, grain size, flow velocity, intact rock mass strength) to help in developing mechanistic models applicable in natural environments.

50 1 Introduction

Continental landscapes evolve through a combination of geomorphological processes, influenced by tectonics and climate. Under inter-glacial conditions, river erosion acts as the primary mechanism responsible for the removal and transport of surface materials. The intricate interplay of various factors, including tectonics, climate, topography, and rock erodibility, contributes to the complex dynamics of river erosion (Whipple, 2004; Whipple et al., 2022; Yanites, 2018). The erodibility of rocks is thought to be modulated by several parameters responsible for river incision, such as the mechanical characteristics of the rocks being eroded, and the size and supply of sediment (Bursztyn et al., 2015; Forte et al., 2016; Jansen et al., 2010; Sklar and Dietrich, 2001; Turowski et al., 2023b; Whipple and Tucker, 1999). However, the efficiency and relative importance of these different parameters in controlling erodibility are not well known (Anderson and Anderson, 2010; Whipple and Tucker, 1999). Experimental approaches can be an attractive approach to address these questions due to slow timescales of erosion and numerous conflating factors that could affect bedrock strength in field settings (Paola et al., 2009). For instance, Sklar and Dietrich (2001) illustrated how sediments in transport and rock strength interact to control the efficiency of bedrock erosion. They demonstrated that erosion rate is maximum with a partial cover of the bed by sediments coarse enough to be transported as bedload. This partial sediment cover provides the tools for abrasion of the bedrock while maximized the rate of sediment impact on the bed surface (Chatanantavet and Parker, 2008; Lague, 2010). Rock properties also play a pivotal role in determining the resistance of bedrock to erosion. All else being equal, lithologies characterized by low tensile strength, such as sandstones or mudstones, tend to erode at higher rates than harder lithologies with higher tensile strength, such as granites or quartzites (Sklar and Dietrich, 2001; Turowski et al., 2023a, b; Zondervan et al., 2020). Lithology and rock fabrics can also influence the dominant erosion process, generally abrasion or plucking, even if cavitation or solution can also matter in some specific conditions (Scott and Wohl, 2018; Whipple et al., 2000b).

Abrasion classically refers to the progressive wear induced by the impact of sediments on the bedrock substrate. This process occurs over extended time scales, creating structures such as ripples, flutes, and potholes, and is thought to lead to lower erosion rates compared to plucking (Anderson and Anderson, 2010; Beer and Lamb, 2021; Whipple et al., 2000b, 2022). In contrast, plucking entails the removal of pre-existing blocks from the fractured bedrock substrate, leading potentially to localized higher erosion rates over shorter time scales (Anderson and Anderson, 2010; Beer et al., 2017; Hurst et al., 2021; Scott and Wohl, 2018; Whipple et al., 2000a; Wilkinson et al., 2018). Previous experimental studies about plucking focus on the flow changes related to plucking of pre-detached blocks (Dubinski and Wohl, 2013; Saha et al., 2021; Wilkinson et al., 2018). They demonstrate that hydraulic forces, including flow contraction, turbulence, and pressure fluctuations, play a critical role on the entrainment and transport of pre-detached blocks in river channels. Because plucking can create sharp changes in bedrock morphology, it is able to induce variations in flow field (via changes in local roughness for example) that may in turn, favors plucking. However, the process of plucking involves two main steps: first, the formation of blocks susceptible to detachment, and second, their removal and transport driven by hydraulic forces (Beer and Lamb, 2021; Chatanantavet and Parker, 2009; Turowski et al., 2023b; Whipple et al., 2000b). The collision of sediments against the bedrock can induce fracturing or damage, thereby promoting the detachment and mobilization of blocks by plucking.

Molnar et al. (2007) and others argue that fracturing of rock by tectonics profoundly decreases their strength, and hence increases their rate of erosion, but also alters their mode of erosion by favouring the occurrence of plucking over abrasion where the bedrock has been fragmented into readily transportable sediments. The classical view is that abrasion dominates in pristine bedrock while plucking tends to prevail and lead to more rapid erosion in highly fractured bedrock (Whipple et al., 2000b; Attal et al., 2006; Hurst et al., 2021; Lima et al., 2021; Scott and Wohl, 2018). Despite the general agreement over this double key role of fractures on erosion processes, few studies have systematically explored the links between fractures and erosion with quantitative approaches. In fact, despite these distinctions, accurately measuring and estimating the relative quantitative contribution of abrasion and plucking to the total erosion rate poses significant challenges (Beer et al., 2017; Whipple et al., 2022). In the following we do not discriminate between joints and faults or between different fracture modes: all mechanical discontinuities, including potentially bedding planes and other geometrical features, are simply referred to as fractures (Eppes et al., 2024).

Recent studies on the role of fractures on erosion have mainly focused on hillslopes (DiBiase et al., 2018; Neely et al., 2019; Neely and DiBiase, 2020). For instance, DiBiase and Neely (2018, 2019, 2020) show that fracturing significantly influences rock erosion, sediment size, and slope of some hillslopes in California. They observe that hillslopes with higher fracture density result in lower relief and smaller sediment blocks, while hillslopes with lower fracture density lead to more pronounced relief and larger blocks. This control of fractures on slopes also has an impact on erosion rates, as the most fractured hillslopes have erosion rates 2 to 5 times greater than less fractured ones (Neely et al., 2019). Regarding rivers, observations in the field indicate that rock fractures significantly impact landscape morphology (Colaianne et al., 2024), influencing both the mode and rate of erosion (Whipple et al., 2000b; Molnar et al., 2007; Scott and Wohl, 2018; Whipple et al., 2022). For instance, it is generally observed that fractured bedrock exhibit wide and rough river channels, while intact bedrock display narrower and smoother channel features (Ehlen and Wohl, 2002; Scott and Wohl, 2018; Wohl, 2008). It is also suggested that river channels may erode faster when the bedrock is highly fractured (Snyder et al., 2003). However, at long time scale, the landscape should equilibrate with the tectonic forces so that these variations in erosion rates might only be transient. By analogy with rock drilling (Thuro, 1997), excavation (Pettifer and Fookes, 1994), or dredging (Vervoort and De Wit, 1997), it is suggested that in bedrock with large fracture spacing with respect to impactors (i.e., sediments), plucking is not favoured and erosion rates seem independent of the presence of fractures (Molnar et al., 2007). Whipple et al. (2000b) also find that plucking dominates abrasion in natural streams when bedrock is fractured over a submeter scale. The dominance of one mode of erosion on the other may influence the morphological differences observed in bedrock rivers (Scott and Wohl, 2018).

Moreover, it was suggested that a continuity of erosion processes operate at different scales, from wear abrasion (i.e., grain-by-grain abrasion) to macro abrasion (i.e., block abrasion by chipping) and plucking (Whipple, 2000b; Whipple, 2004; Beer and Lamb, 2021). This is supported by laboratory experiments showing the scaling over 13 orders of magnitude of the abraded volume with the impactor's kinetic energy, normalized by the tensile strength of the impacted bedrock (Beer and Lamb, 2021). Under both abrasion regimes, and assuming that fractures preferentially develop along pre-existing boundaries in bedrock, such as contacts between minerals, it is postulated that erosion is more efficient when the impactor size is similar to the size of the minerals constituting the bedrock, allowing to maximize the impact energy delivered to unit boundaries (Turowski et al., 2023b). Similarly, in most cases, plucking can only occur after a phase of fracture propagation to finish individualizing a pluckable block or to disintegrate an initial large block into smaller and more easily mobilized ones. This is favoured by hydraulic forces (e.g., drag and lift, differential pressure between the block surface and its basal fracture), elast wedging and impact of coarse sediments (e.g., Whipple, 2000b). In addition to fracture propagation, the impact of coarse sediment also probably plays a large role in tilting and lifting the already individualized block out of its initial position. The differences between macro abrasion and plucking can therefore become scarce or confusing, as in both cases fractures play a key role and eroded fragments can be similarly large. In a general way, plucking can be defined as the mobilization of bedrock blocks under

the combined action of hydraulic forces and impacting sediments. In the following, we focus on plucking occurring by both mechanisms, when blocks are not fully available for transport.

Based on this last definition, our study investigates how the geometry of rocks with mechanical discontinuities affects the magnitude, location and the dominant mode of erosion, by plucking or abrasion. We conduct laboratory experiments inspired by Sklar and Dietrich (2001), considering an additional variable: the fracture network geometry. Artificial concrete stones with different fracture networks are eroded in mills with constant flow speed and sediment mass. We monitor the evolution of the topography at regular time intervals and derive erosion rates from topographic differences. We evaluate how the fracture geometry controls the capacity to erode by plucking compared to abrasion, and thus the local and short-term erosion rate shaping the topography.

River incision into bedrock is a key process in continental landscape evolution, the efficiency of which is modulated by discharge statistics, channel geometry, sediment supply, and rock mechanical properties (Lague, 2014; Whipple, 2004; Whipple et al., 2022; Yanites, 2018). Developing long-term incision laws accounting for these factors using mechanistic-based arguments is a long-standing challenge in quantitative geomorphology (Whipple et al., 2022). Among key advances, Sklar and (2001) seminal experiments have shown that for homogeneous rocks, the efficiency of erosion by saltating bedload decreases as the inverse square of the rock tensile strength. This experimental result was later confirmed with different materials, extended to suspended load (Scheingross et al., 2014), and has been central in building a mechanical understanding of the link between bedrock lithology and erosion efficiency (e.g., Chatanantavet and Parker, 2009; Sklar and Dietrich, 2004). However, in nature, rocks are frequently fractured, bedded, or contain joints that create mechanical discontinuities that are expected to alter erosion efficiency compared to a homogeneous intact rock. While there have been attempts at considering this effect in bedrock incision models (Chatanantavet and Parker, 2009; Whipple et al., 2000b), we are far from being able to include quantitatively the effect that mechanical discontinuities have on erosion efficiency and long-term bedrock incision.

Away from waterfalls and debris-flow-dominated reaches, erosion processes that drive river incision into rocks with mechanical discontinuities are classically sub-classified into two categories (Whipple et al., 2022): abrasion and plucking processes. Here, we only consider rivers transporting coarse bedload material, typical of actively eroding mountain belts, and in rock lithologies where dissolution is negligible. Abrasion refers to the progressive wear induced by the impact of sediments on the bedrock substrate (Hancock et al., 1998; Sklar and Dietrich, 1998; Whipple et al., 2000b). This process can operate at different scales from wear abrasion (i.e., grain-by-grain abrasion) to macroabrasion. Macroabrasion is a recent terminology encompassing a variety of mechanical processes: chipping of blocks by grains (Beer and Lamb, 2021; Hancock et al., 1998; Whipple, 2004); breaking of bedrock into blocks by the impact of large clasts (Scott and Wohl, 2019); progressive fracturing of the bedrock surface through repeated impacts creating rock fragments that can then be subsequently entrained (Chatanantavet and Parker, 2009, 2011). Macroabrasion does not necessarily require pre-existing rock mass discontinuities. On the contrary, plucking occurs and is described in the context of rocks having pre-existing discontinuities such as fractures, joints, or bedding (Whipple et al., 2022). A detailed review of the literature shows that the exact processes encompassing plucking differ among authors. Some consider it as the process of removing blocks that are already completely loose by hydraulic forces (Saha et al., 2021; Scott and Wohl, 2019), with a variety of processes involved, such as sliding (Dubinski and Wohl, 2013), vertical lifting (Wilkinson et al., 2018), and toppling (Lamb and Dietrich, 2009). Others describe plucking as a two-step process (Beer et al., 2017; Chatanantavet and Parker, 2009; Whipple, 2004; Whipple et al., 2000b). First, the formation and loosening of blocks susceptible to detachment (e.g., by weathering, macroabrasion, hydraulic jacking or wedging), and second, their entrainment by hydraulic forces (Beer and Lamb, 2021; Chatanantavet and Parker, 2009; Turowski et al., 2023; Whipple et al., 2000a, b). A typical example of the second definition is the progressive impact-driven creation of cracks between pre-existing fractures to create loose blocks that are subsequently entrained (e.g., fig. 4A in Whipple et al 2022, itself derived from fig. 4 in Whipple et al 2000b). Hydraulic wedging and jacking by transported grain can both help in crack development as well as entrainment (e.g., Hancock et al., 1998; Hartshorn et al., 2002). In this study, we adhere to this second

170 definition of plucking. We note that glacial erosion by plucking (also called quarrying) is also defined as a similar 2 steps
process encompassing a weathering/fracturing phase and an entrainment phase (Anderson and Anderson, 2010; Hallet, 1996;
Scott and Wohl, 2019). Beyond semantics, we note that a key point is that a larger range of erosion processes encompassing
wear, macroabrasion and plucking can occur in rocks with mechanical discontinuities, compared to homogeneous rocks. This
makes quantifying the impact of discontinuities on erosion efficiency a challenging problem (Scott and Wohl, 2019) as the
proportion and the rate of each process must be quantified.

175 The empirical expectation is that if discontinuities are close enough, plucking tend to prevail over abrasion and yield higher
erosion efficiency (e.g., Attal et al., 2006; Hurst et al., 2021; Lima et al., 2021; Molnar et al., 2007; Scott and Wohl, 2019;
Whipple et al., 2000b). As the spacing of discontinuities increases, plucking is expected to become too infrequent to become
a dominant mechanism even though large blocks can be removed at once and contribute massively to long-term erosion (e.g.,
Beer and Turowski, 2015; Hancock et al., 1998; Whipple et al., 2000b). Field observations indicate that rock fractures, joints,
180 and bedding significantly impact channel morphology (e.g., Hancock et al., 1998; Lima et al., 2021; Whipple et al., 2000b).
For example, fractured bedrock is generally associated with rougher river channels, where plucking dominates, whereas intact
bedrock tends to form smoother channels, dominated by abrasion (Ehlen and Wohl, 2002; Lima et al., 2021; Scott and Wohl,
2019; Wohl, 2008). Beyond fracture density, fracture dipping and orientations can influence how easily blocks are removed
from bedrock (Scott and Wohl, 2019), with downstream-dipping fractures favouring sliding or pivoting and upstream-dipping
185 fractures creating more resistance to erosion (Wohl, 2000). Beyond the intuition derived from field-derived morphological
constraints informing on the nature and relative dominance of various processes (Whipple et al., 2000b), very few studies have
been able to directly quantify it in situ. Hartshorn et al. (2002) documented annual rates of erosion across a bedrock channel
for two lithologies with a 4-time difference in tensile strength. Yet owing to jointing, the more resistant rock was eroding
through plucking much faster than the weak one, dominated by abrasion. Beer and Turowski (2015) used 3D scans to
190 systematically document patterns of abrasion in a gorge incised in mostly massive rock and showed that a single large plucking
event, during their 2-year survey period, accounted for one-third of the total erosion. They underlined the difficulty in
accounting for the fundamental stochastic nature of plucking (e.g., Snyder et al., 2003) and in assessing the contribution of
extreme events and the impact of very large boulders in driving macroabrasion on massive rocks. Lastly, experimental studies
provide important insights into the mechanics of bedrock incision (e.g., (Beer and Lamb, 2021; Dubinski and Wohl, 2013;
195 Paola et al., 2009; Scheingross et al., 2014; Sklar and Dietrich, 2001; Turowski et al., 2023; Wilkinson et al., 2018; Wilson
and Lavé, 2014)). Yet, no experimental setup has been developed that would combine both abrasion and plucking processes
at the same time. Similarly, numerical models that could couple complex flow hydraulics, sediment transport, and rock
mechanics have not yet been developed. Hence, we are still lacking a clear understanding of how fracture geometry influences
bedrock river erosion processes and rates, and methods to explore this question.

200 To progress on this knowledge gap, we have developed a new erosion mill experiment inspired by the setup of Sklar and
(2001), considering an additional variable: a network of discontinuities mimicking fractures with a controlled geometry that
we can vary. Our artificial bedrock is made of concrete with 3D printed fracture patterns acting as planar discontinuities. The
parameter space potentially controlling erosion efficiency in this setup is large, as we can control flow velocity, sediment load,
sediment size, and the fracture pattern. In this first study, we only explore the effect of the fracture pattern and keep the other
205 parameters constant. Experiments with a purely homogeneous concrete serve as a reference case where only abrasion occurs,
as in Sklar and Dietrich (2001). We reconstruct precisely the topographic evolution at regular time intervals and use this
information to quantify spatial patterns of erosion, erosion statistics, and the dominant mode of erosion. When a fracture exists,
we use the dual classification of plucking vs abrasion in separating large block detachment detected from erosion patterns,
from smaller local topographic change corresponding to abrasion. However, one objective of this study is to characterize the
210 nature of the processes driving erosion in this new material, including the potential occurrence of macroabrasion when fractures
exist. The work is organized as follows: we first present the new experimental setup and the design choices for the artificial

fractured bedrock. We then present the results focusing on the role of fracture density, spacing, and dip in controlling mean erosion rates, the relative contributions of plucking and abrasion, and the size distribution of plucking events. The discussion then addresses the benefits and limits of this new setup, the dominant erosion processes and the relevance of our experimental results to natural systems.

2 Methods and materials

The experimental setup consists of an erosion mill system, inspired by previous designs (Sklar and Dietrich, 2001). It features a Plexiglas column with a fractured concrete disk positioned at the bottom. For the experiment, we use the terminology “fracture” to describe a mechanical discontinuity of planar geometry with a resistance lower than the intact concrete disk. Sediments and water are placed above the disk, while a rotating propeller generates sediment motion, driving the erosion process.

2.1 Experimental disks

Our fractured substrates are simulated with a synthetic mesh placed in a circular mould before pouring concrete disks. Each network is made up of two families of fractures with different spacing and dip angles (Fig. 1a). First, we perform experiments with square networks (i.e., the two families have the same spacing) and vertical fractures. We use three different spacings (10, 20, and 40 mm) and repeat the experiments at least twice to account for intrinsic variability. Then, we perform experiments with rectangular networks (i.e., the two families have different spacings) and vertical fractures. We tested two configurations (10/20 and 10/35 mm) and repeated one of them (the 10/20 mm) to assess reproducibility. Finally, we perform experiments to explore the influence of the fracture dip angle, which represents the angle between the fracture plane and the horizontal plane. Starting from a square network of fractures spaced by 20 mm, we change the dip angle of either one or the two both fracture families. We use two symmetrical networks (45/45 ° and 67/67 °) and repeat at least twice each experiment, and three asymmetrical networks (45/67 °, 90/45 ° and 90/67 °) that we did not repeat. In total, we used 10 different networks and ran 19 experiments with fracture networks. Different methods have been proposed to describe and characterise networks of fractures in natural rocks (e.g., Eppes et al., 2024). Here, the geometry is quite simple, and we therefore only use two parameters: the fracture density, referred to as p_{21} and defined as the total length of fractures visible on the surface over a given area (Dershowitz and Herda, 1992), and the sum of the fracture dip angles to distinguish the experiments with similar spacing but different dip angles. The experiments and their geometrical properties are summarized in Table 1.

We use OpenSCAD to model the fracture networks in 3D and a ZORTRAX M200 3D printer to print them, with a fracture width of 0.9 ± 0.1 mm. To create weak zones inside the concrete disk without impeding its erosion, fractures, fracture

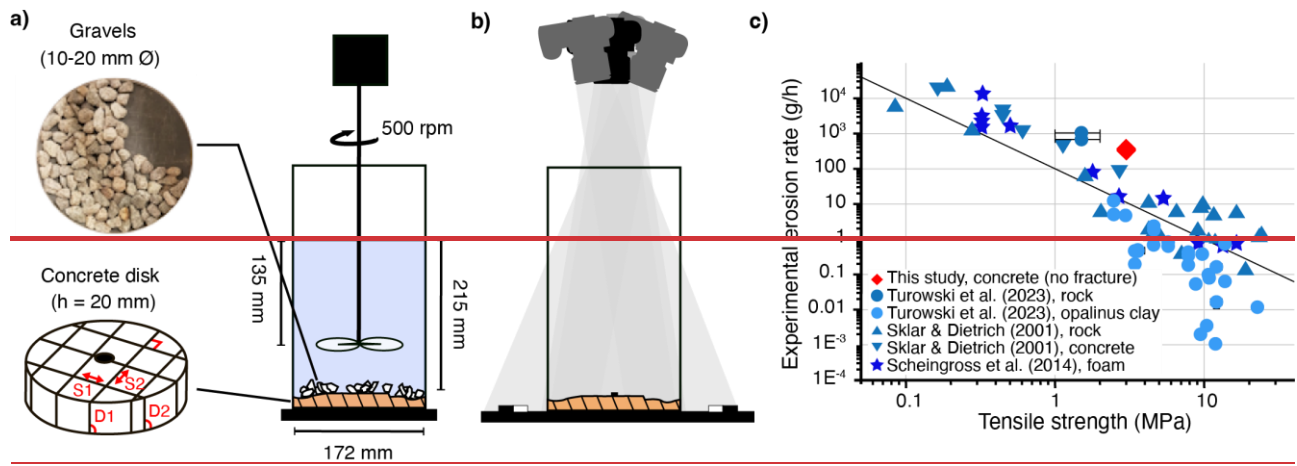


Figure 1: General design of the experiments with a) the setup with the geometric parameters of the fracture networks that we explore in this study (with S and D the spacing and the dip angle of the two families of fractures, respectively), and b) the photogrammetry system. The concrete disk is fixed at the bottom of the column and erosion is launched by the motion of the water and gravels induced by the propeller. Every 2 minutes, the column is emptied and placed under 4 cameras. Targets are placed in the scene for absolute scale. c) Average erosion rate according to the tensile strength for various erosion mills (blue symbols) and for our concrete without fracture (red diamonds) (adapted from Turowski et al, 2023).

networks are first printed using white BVOH (Butenediol Vinyl Alcohol Co-polymer), a thermoplastic that normally fully dissolves or becomes soft in water. Yet, when in contact with cold water-cement during, the BVOH softens, but does not fully dissolve. This results in a network of mechanical discontinuities with much lower strength than the intact concrete, while maintaining a minimal cohesion of the disk, as fractures are not empty. Once printed, we use the fracture network is placed in a circular mould (diameter = 172 mm, height = 20 mm) to pour, and concrete is poured over the printed network-it. Attempts to create a fully 3D fractured network with holes that would allow cement to fill in the void inside the mesh were unsuccessful. We thus kept using only 2 sets of fracture planes that extend from the top to the bottom of the disk. For experiments without fractures fracture networks, the concrete is directly poured into the mould. We insert a 1.5 mm diameter plastic tube in the center of the mould so that we can fix the disk on the column with a screw during the experiment. The concrete mix proportioning consists in of one part of cement (CEM II/B-LL 32,5 N), three parts of Fontainebleau sand ($D_{50} = 210 \mu\text{m}$ and $D_{\text{max}} < 350 \mu\text{m}$), and 15 % of water in weight. This composition was selected to ensure that the concrete disk erodes at a moderate rate—slow enough to track topographic evolution but fast enough to complete each experiment within a few hours. Concrete disks are carefully removed from the mould after 3 days and left to harden for an additional 5 days in an airtight box. The disk is then slightly sanded to make it as flat as possible and fixed at the bottom of the Plexiglas column. In our setup, the blocks are only pre-made by the vertical fractures. The third join, at the bottom, has to form in situ before any block can be entrained in the flow. In addition, the fractures correspond to localized contrast in rheology but the disk is still cohesive. In consequence, when plucking occurs, the involved area may follow the fractures but it can also be different. All these operations require extreme caution as the fractured disks are extremely fragile and can easily break along fracture plans even before the BVOH is further softened by immersion in the tank. This fragility explains why we cannot run mechanical tests on the fractured disk. Similarly, because the BVOH mechanical behaviour is altered by the cement, we cannot estimate the exact mechanical properties of the fractures when the BVOH has softened. Once immersed in the water, a fractured disk cannot be removed as it breaks instantaneously.

In our setup, the 2 sets of fractures delimit blocks spanning from the top to the bottom of the concrete disk. The major third horizontal joint is the interface of the disk with the base of the tank. As will be shown in the results, plucking of complete blocks can occasionally happen towards the end of experiments; however, plucking occurs principally through horizontal crack development at various depths between preexisting fractures due to grain impacts. An objective of this study is to characterize this process and evaluate the potential contribution of macroabrasion.

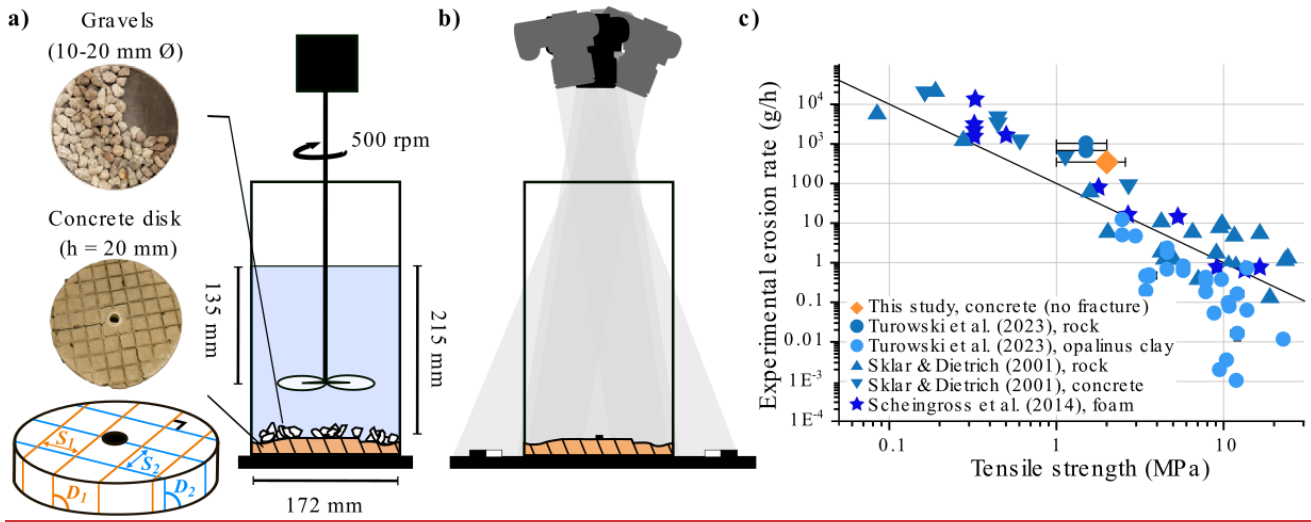


Figure 1: General design of the experiments with a) the setup with the geometric parameters of the fracture networks that we explore in this study (with S and D the spacing and the dip angle of the two families of fractures, respectively), and b) the photogrammetry system. The concrete disk is fixed at the bottom of the column and erosion is launched by the motion of the water and gravels induced by the propeller. Every 2 minutes, the column is emptied and placed under 4 cameras. Targets are placed in the scene for absolute scale. c) Average erosion rate according to the tensile strength for various erosion mills (blue symbols) and for our concrete without fracture (orange diamonds) (adapted from Turowski et al. 2023).

To characterize our intact concrete, we estimate ~~theits~~ tensile σ_t and compressive σ_c strengths ~~of our concrete at after~~ 28 days of drying. Tests are performed on prismatic samples referring to EN 196-1 (EN 196-1:2016 | May 2016, Methods of testing cement – Determination of strength) (AFNOR, 2016). We also estimate the mechanical properties of four additional concretes made with the same cement to sand ratio but with different water content (-20 %, -10 %, +10 % and +20 % with respect to the reference concrete), Supplementary material S1). Despite these differences, the five concretes exhibit similar properties, with $\sigma_t = 3.01 \pm 0.04$ MPa and $\sigma_c = 10.11 \pm 0.50$ MPa. All experiments were made within this range of water content. For such mixes, the F eret relationships (F eret, 1892) relate their mechanical properties to their composition:

$$\sigma_c = G \cdot \sigma_{ccf} \cdot \left(\frac{v_c}{v_c + v_w + v_a} \right)^2 = G \cdot \sigma_{ccf} \cdot (c)^2 \quad (1)$$

$$\sigma_t = G' \cdot \sigma_{ctf} \cdot \left(\frac{v_c}{v_c + v_w + v_a} \right) = G' \cdot \sigma_{ctf} \cdot c \quad (2)$$

with v_c , v_w and v_a the volume of cement, water and air per unit volume of concrete, respectively. G and G' act as granular coefficients. The compressive σ_{ccf} and Because we perform experiments after only 7 days of drying, the tensile σ_{ctf} strengths at 28 days strength is expected to be lower than the measured on the cement with standard sand (EN 196-1) serve as indicators of the cement quality. For the selected cement, the values at 28 days, are $\sigma_{ccf} = 20$ MPa and $\sigma_{ctf} = 4.4$ MPa. Consequently, for Fontainebleau sand, $G = 4.9$ and $G' = 2.1$. The mechanical performances of mixes appear directly linked to the compacity c of the paste (cement + water + entrapped air). While an increase in v_w affects c , it also enhances the workability of the mix, reducing the amount of entrapped air. Interestingly, the reduction value. Using information from the Bulletin du Ciment (1950–1951), we estimate this value at 2 MPa with a conservative uncertainty of 1 MPa. Compared with existing abrasion mill experiments (Fig. 1c), this places our concrete in air volume compensates for the additional water, resulting in minimal changes to the mechanical strengths of the concrete within the studied an intermediate range of water content (Fig. S1). between very weak material (~ 0.1 MPa) and very resistant rocks (> 10 MPa).

2.2 Experimental protocol

For each experiment, the disk fixed at the bottom of the Plexiglas column is immersed in water until saturation of the connected porosity, which occurs in about 20 minutes. To induce erosion, we add a constant volume of water together with

granitic gravels of 10-20 mm in diameter on the top of the disk. To maximize erosion rates, the sediments cover about 2/3 of the surface of the disk at rest (Sklar and Dietrich, 2001, Fig. 1a). Sediments are weighed at regular time intervals to ensure their mass remains constant. In only a few experiments, we added one grain during the run to keep the mass constant.

~~The rotation rate of the propeller placed in the column is 500 rpm so that the maximal flow speed at the edges of the column is of a few meters per second, and the sediment motion induces erosion by abrasion and plucking. Every 2 minutes, we stop the propeller, remove the water and the sediments, and take 4 pictures of the disk surface with fixed and remotely triggered cameras (Fig. 1b). During the experiments, parts of the disk can be removed by plucking (after the third joint set has formed) and become part of the sediment load. However, these concrete blocks are lighter and weaker than the granite grains, and we assume that they do not contribute significantly to erosion. To maintain a constant sediment mass, we remove all visible concrete fragments after each 2 minutes time interval. An experiment ends when the bottom of the plexiglass column is reached, which corresponds on average to half a day per experiment and to about 60 minutes of effective erosion. For each experiment, we thus get 30 to 40 time steps. Such test duration appears sufficiently short to neglect the concrete strengths increases due to the continuous hardening of the cement.~~

~~The rotation rate of the propeller placed in the column is 500 rpm, so that the maximal flow speed at the edges of the column is a few meters per second, and the sediment motion induces erosion. The propeller is 3D printed, and we tested various designs to limit the vertical recirculation cell that is documented in previous mill experiments (e.g., Sklar and Dietrich, 2001; and Small et al., 2015). The objective was to have a simpler radial velocity gradient with maximum abrasion near the mill edge rather than away (e.g., nearly 50 mm in Small et al., 2015). We note that erosion does not occur if sediment is not included. Every 2 minutes, we stop the propeller, remove the water and the sediments, and take 4 pictures of the disk surface with fixed and remotely triggered cameras (Fig. 1b). During the experiments, fragments of the disk can be removed by plucking and become part of the sediment load. However, these concrete blocks are less dense and weaker than the granite grains, and we assume that they do not contribute significantly to erosion. To maintain a constant sediment mass, we remove all visible concrete fragments after each 2-minute time interval. An experiment ends when the bottom of the plexiglass column is reached, which corresponds on average to half a day per experiment and to about 60 minutes of effective erosion. Once we reached this stage, it became impractical to continue the experiment, as we cannot easily remove the water and sediment, as the whole disk disaggregates quickly. For each experiment, we thus get 30-to 40-time steps. Such a test duration appears sufficiently short to neglect the concrete strength increases due to the continuous hardening of the cement.~~

We reconstruct the topography of the disks using photogrammetry with Agisoft Metashape, generating point clouds with elevation (z) and horizontal coordinates (x, y). Since the four cameras remain fixed throughout the experiment, we use the 4D mode (i.e., a temporal series from fixed cameras), ensuring that the disks are consistently referenced in the same position.

To establish an absolute spatial scale, we place reference targets with known locations around the disk, which are automatically identified by the software. After reconstructing the topography as point clouds, we use the Canupo classification algorithm (Brodu and Lague, 2012) (Brodu and Lague, 2012) to filter out points classified as noise (mainly due to reflections on the Plexiglas tube), ensuring a cleaner and more accurate dataset. The remaining point clouds have a resolution of a few points per millimetre. Then, to obtain erosion maps from the topographies, we use the M3C2 algorithm (Lague et al., 2013) in a vertical model to calculate the differences in elevation between successive pairs of point clouds. We use a regular grid of core points with one point per millimetre so that each cloud has about $21,000 \pm 1000$ points. The projection scale in M3C2 is 2 mm, resulting in an average of 25 points from each cloud used to compute the vertical difference.

To quantify the uncertainty associated with topographic reconstruction and point cloud differencing, we repeat ~~10 times~~ this protocol 10 times with the same disk saturated with water (i.e., removing and replacing the column, taking pictures, generating the point cloud, and 3D point cloud differencing). The maximum local difference in elevation between the 10 point clouds is 0.15 mm, and we use this value as the topographic uncertainty in the following.

For practical reasons, we then convert the point clouds to rasters with 1 mm of resolution describing the elevation of the topographic surfaces $z(x, y)$, the M3C2 differences $\Delta z(x, y)$ and the erosion rates $\Delta z(x, y)/\Delta t$, with Δt the duration between two acquisitions (i.e., 2 minutes). In addition, at each time step, we weight the column after removing the water and the grains. These mass measurements only give a value averaged over the whole surface of the disk and are therefore less detailed than the topographic measurements. Therefore, they are only used to ~~control~~ensure that we accurately capture the erosion dynamics from the topographic evolution. ~~It is important to note that our results depend on the rheology of the materials we used in the experiment.~~

~~To compare our material to the ones from previous similar experiments (Turowski et al., 2023a), we run 4 experiments with no fractures and weight the column every 2 minutes to estimate the average erosion rates. Values are similar between the four experiments and match well with previous data (Fig. 1c). These experiments serve as a reference for the behaviour of our concrete without any fracture.~~

~~To compare our fractured material to homogeneous cases, we run 4 experiments with no fractures. Using the weight data measured every 2 minutes to estimate the average erosion rates. Average erosion rates derived from weighing the column every 2 minutes are similar between the four experiments and match well with previous studies (Fig. 1c, Scheingross et al., 2014; Sklar and Dietrich, 2001; Turowski et al., 2023).~~

2.3 Data analyses

For each experiment, we derive two erosion rates from the erosion maps: i) the mean erosion rate, corresponding to the average erosion of the disk for each time interval, and ii) the local erosion rate, corresponding to the erosion at each point of the raster and for each time interval. The mean erosion rate calculated from topographic differences correlates well with the weight measurements (Fig. S2S3). The average erosion rate for each experiment is defined as the mean of the mean erosion rates, and we use one standard deviation as the associated uncertainty.

In this study, we use the term plucking for any localized event of high-intensity erosion (i.e., more intense than the background erosion by abrasion). For each plucking event, we extract its location, area, volume (defined as the area times the change in elevation between the consecutive topographies) and time of occurrence, and we define the proportion (in %) of erosion by plucking with respect to total erosion as the ratio between the sum of erosion by plucking events during the whole experiment and total erosion. ~~The size of the blocks is influenced but not set by the fractures as 1) the area in surface can follow or not the fractures and 2) the 3rd join has to form in situ before a block can be removed.~~

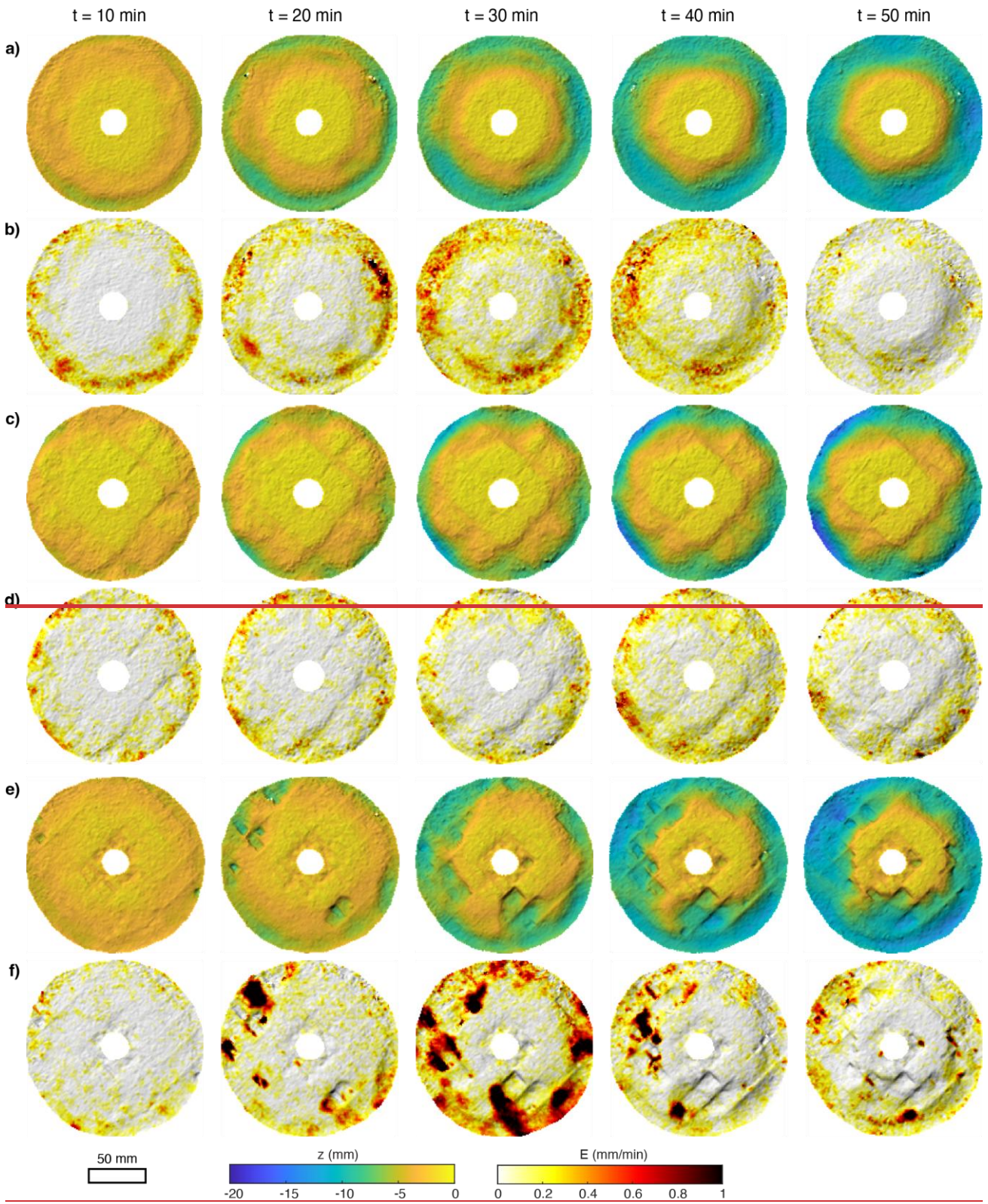


Figure 2: Temporal evolution of the topography and erosion rates of three different experiments. The first disk (a, b) has no fracture, the second (c, d) has a moderately dense network ($p_{z1}=50 \text{ m}^{-1}$, corresponding to vertical fractures with a spacing of 40 and 40 mm) and the third one (e, f) has a dense network ($p_{z1}=145 \text{ m}^{-1}$, corresponding to vertical fractures with a spacing of 10 and 20 mm). The time step between two pictures is 10 minutes. The full temporal series (i.e., topography and erosion maps every 2 minutes) of these three experiments is available in the Supplement Material Fig. S5

3 Results

In this section, we first explore the impact of fracture density by focusing on experiments with vertical fractures only. In the second part of this section, we investigate the role of the fracture dip angle by focusing on experiments with fixed spacing (20/20 mm) but variable dip angle.

3.1. The topographic evolution of experiments is linked to fracture densities

During an experiment, the topography of the disks evolves due to erosion, and we observe distinct patterns with and without fractures, illustrated in Figure 2 (the full temporal series, i.e., topography and erosion maps every 2 minutes are provided as Supplement Material, Fig. S5). In experiments with no fracture ($p_{21} = 0 \text{ m}^{-1}$), we observe a) erode via continuous wear of the topography through time with a clear radial pattern (Fig. 2a, S5a-S6a). At the end of a run, the topography is quite smooth and exhibits a radial symmetry. Indeed, the central part of the disk is eroded less while, with about 1.5 mm of material is removed near the edge. This radial pattern is due to the rotative flow that induces a centrifuge force, pushing the grains toward the edge and generating a higher flow velocity and shear stress near the disk edge. Overall, this leads to a more frequent and more energetic impact of grains near the disk edge. In the experiment shown in Fig. 2a, the average erosion rate is $0.16 \pm 0.04 \text{ mm/min}$ (Table 1) and is characterized by a strong radial gradient, going from about 0 mm/min at the centre of the disk to about 0.6 mm/min on the edge (Fig. 2b, S5b). This behaviour (i.e., a smooth topography with radial symmetry and a radial pattern of erosion rates with limited intensity) is typical of experiments dominated by abrasion. AS6b). The erosion map shows localized patches of higher erosion rate, 2 to 3 times larger than the average erosion rate, and extending over a maximum of 2 cm. They tend to occur in the inner side of the trough created by the previous erosion and correspond to a progressive inner expansion of the active incision zone. A broadly similar behaviour is observed in experiments with a limited number of fractures ($p_{21} = 50 \text{ m}^{-1}$). In such experiments, the influence of the fractures is visible in the topography (Fig. 2c, S5c) and we sometimes observe spots of high erosion rates located near the fractures (Fig. 2d, S5d). They correspond S6c), leading to small plucking events but due to their limited size, they do not significantly modify the topographic evolution with respect to experiments with no fracture at all. a less regular radial pattern. The average erosion rate is slightly lower ($0.14 \pm 0.03 \text{ mm/min}$, Table 1) than in the absence of fractures, but within the range of uncertainties. On the contrary, experiments with a dense network ($p_{21} = 145 \text{ m}^{-1}$) show a different topographic evolution. We still observe a radial pattern related to abrasion, is still present with more erosion on the edges than in the centre (Fig. 2e, S5e). Yet, S6e), but the topography is more irregular with sharp changes in elevation changes. Erosion is no longer symmetrical nor regular through time, and we observe patches of high erosion rates, up to 1 mm/min, are located all over the disk (Fig. 2f, S5f). They S6f), bounded laterally by the fracture pattern. When emptying the column, we find concrete debris, some of them with sizes corresponding to the fracture pattern and is a few mm thick (see section 3.5 for a detailed analysis of the debris sizes). This shows that at least some of the high erosion patches correspond to sudden removals of blocks (i.e., instantaneous plucking events) and their size relates to the spacing of the from cracks that have developed horizontally between fractures. The average erosion rate is only slightly higher than without fractures ($0.17 \pm 0.05 \text{ mm/min}$, Table 1). In these experiments, abrasion and plucking coexist and lead to these specific patterns: an irregular topography with erosion over a large surface and superposition of locally high erosion rates on top of a radial pattern of erosion. In all As for previous experiments, we observe that erosion occurs first on the edges of the disks before to progress progressing inward (Figs. 2a, 2c, 2e, S5a, S5e, S5e-S6a, S6c, S6e).

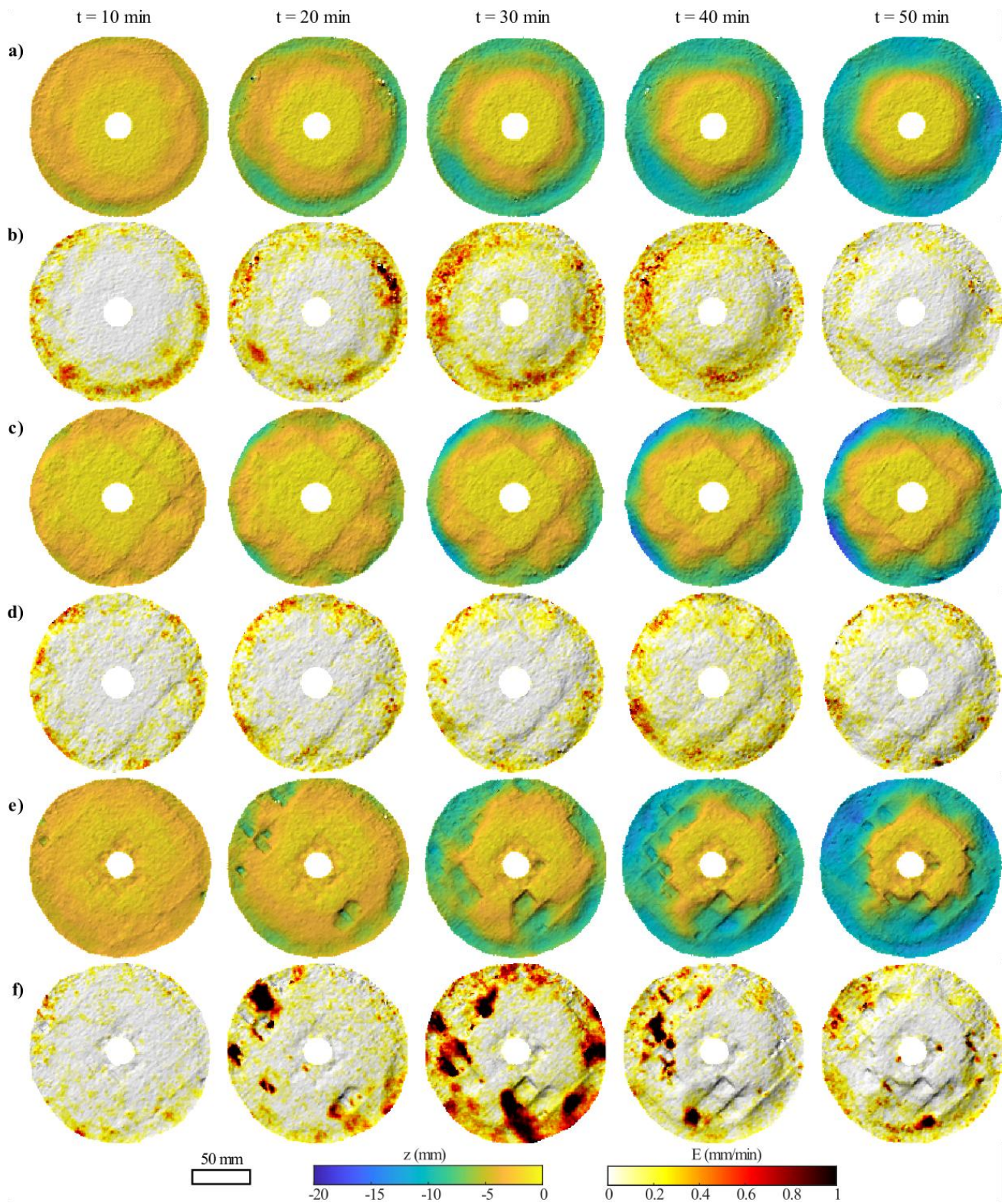


Figure 2: Temporal evolution of the topography and erosion rates of three different experiments. The first disk (a, b) has no fracture, the second (c, d) has a moderately dense network ($p_{21}=50 \text{ m}^{-1}$, corresponding to vertical fractures with a spacing of 40 and 40 mm) and the third one (e, f) has a dense network ($p_{21}=145 \text{ m}^{-1}$, corresponding to vertical fractures with a spacing of 10 and 20 mm). The time step between two pictures is 10 minutes and the flow direction is clockwise. The full temporal series (i.e., topography and erosion maps every 2 minutes) of these three experiments is available in the Supplement Material Fig. S6.

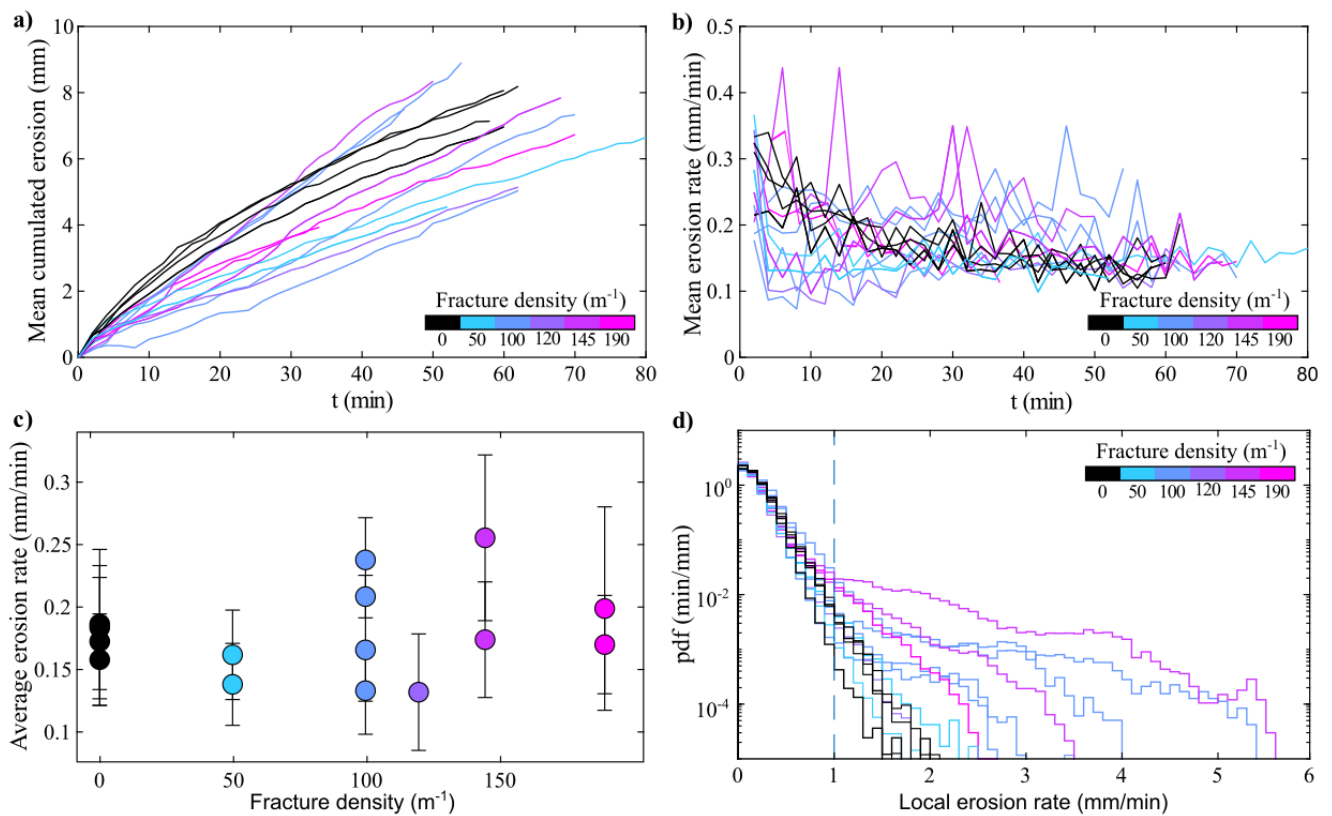


Figure 3: Erosion through time of the different disks with: a) the cumulated erosion (in mm) and b) the mean erosion rate (mm/min). The bold curves correspond to the disks of Fig. 2. Distribution of c) the average erosion rates and d) the probability density function of the local erosion rates.

3.2 Average and local Temporal evolution of erosion rates are barely controlled by and the influence of fracture density or spacing

Having such a detailed temporal series evolution of the mean cumulated erosion maps is quite unusual (Fig. 3a) and we make use of this opportunity to investigate the temporal evolution of the mean erosion rate for each experiment. Here, we only focus all experiments (Fig. 3b) show two types of evolution depending on experiments with vertical the presence of fractures and compare them against. For unfractured experiments with no fractures:

Despite obvious differences in topography and erosion dynamics, we observe a roughly similar temporal evolution of the mean cumulated erosion for all experiments (Fig. 3a). More variability is revealed when considering the mean erosion rate (Fig. 3b). During the first 10 to 20 minutes is of the order of 0.3 mm/min at first and then decreases progressively towards a steady value of about 0.13 mm/min reached around 30 min, with fluctuations typical of the uncertainty in the 3D measurement approach (0.075 mm/min). For fractured experiments, the mean erosion rate tends to decrease before stabilizing between 0.1

and 0.2 mm/min (Fig. 3b, Table 1). Large shows very large variations are observed in experiments with fractures, with mean rates up to 0.4 mm/min. These 45 mm/min. Through the comparison with the map of erosion rates (Fig. 2), we observe that the high peaks in mean erosion rate (Fig. 3b) are associated with large plucking erosion events occurring over the specific time step. For example, the sudden increase observed peak of 0.35 mm/min occurring at 30 minutes on the bold purple line around 30 minutes in (Fig. 3a and 3b) corresponds to the large plucking event visible in Fig. 2f. We observe also some variability in experiments without fractures, which suggests that abrasion shows some stochasticity. In addition, we observe no specific

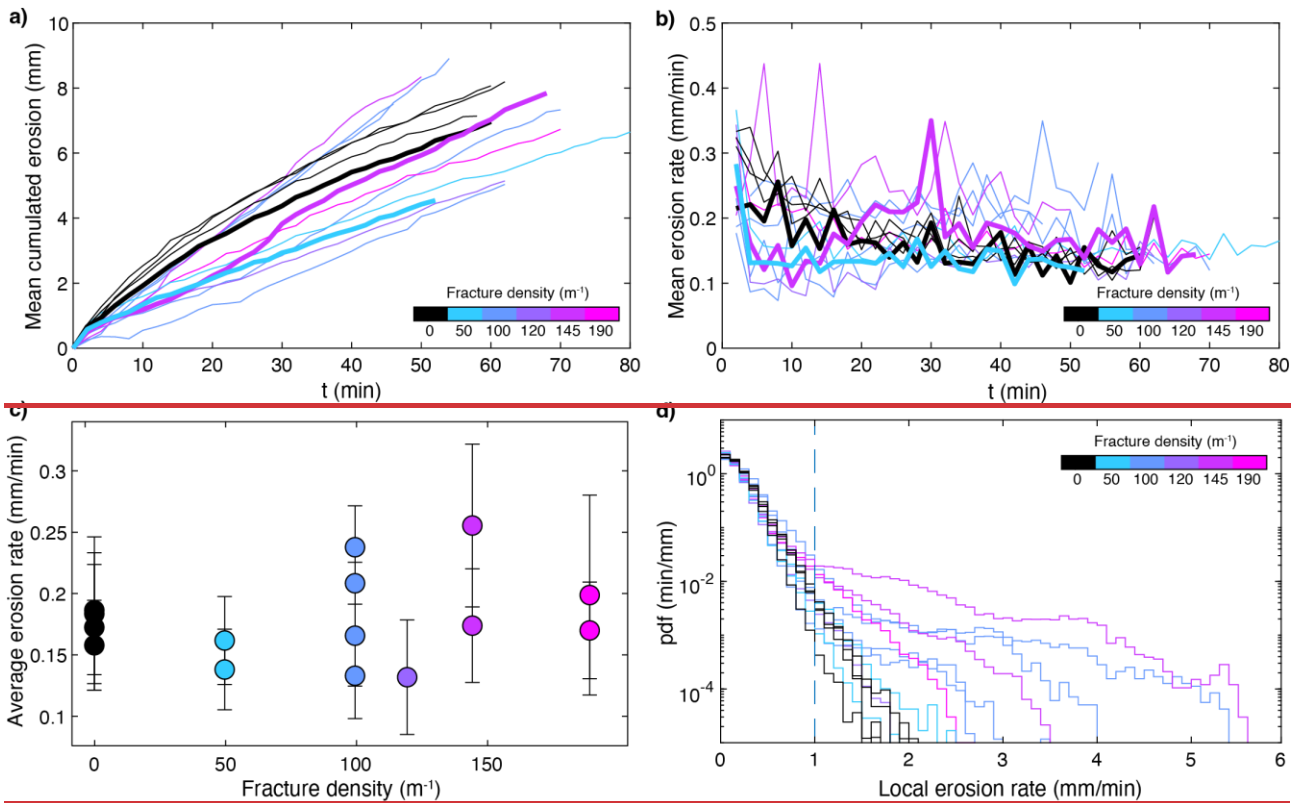


Figure 3: Erosion through time of the different disks with: a) the cumulated erosion (in mm) and b) the mean erosion rate (mm/min). The bold curves correspond to the disks of Fig. 2. Distribution of c) the average erosion rates and d) the probability density function of the local erosion rates.

trend with respect to the fracture density on the cumulative erosion and the mean erosion rate (Fig. 3a and 3b). These results indicate that, in our experiments, The cumulated erosion curve shows that unfractured experiments have eroded faster for the first 20 minutes than any of the fractured experiments. Even if fractured experiments show a very high variability of mean erosion rates, the cumulated erosion rate tends to increase linearly with time, showing that there is no clear reduction of the mean erosion rate through time as in unfractured experiments. The cumulated erosion rate curves also show that 3 (resp. 7) fractured experiments have higher (resp. lower) cumulated erosion at the end of the experiment than unfractured ones. Beyond the different temporal dynamics between the fractured and unfractured experiments, we do not observe an obvious relationship between the fracture density and the total cumulated erosion rate or the mean erosion rate does not discriminate between experiments with or without fractures. temporal evolution.

Rather than looking at the experiments separately, we now group them according to their Comparing average erosion rates, averaged over the entire simulation duration, to fracture density and look at the average erosion rates (calculated as the mean of the mean erosion rates shown in confirms the lack of clear dependency (Fig. 3b). For the 11 experiments presented here, the3c). The average erosion rates range from 0.13 ± 0.05 mm/min ($p_{21} = 120$ m⁻¹) to 0.26 ± 0.07 mm/min ($p_{21} = 145$ m⁻¹). We observe some variability between experiments performed with the same network, however it is-) and are all within the one standard deviations (Table 1) so that the variation in mean erosion rate during one run is larger than the variation between two

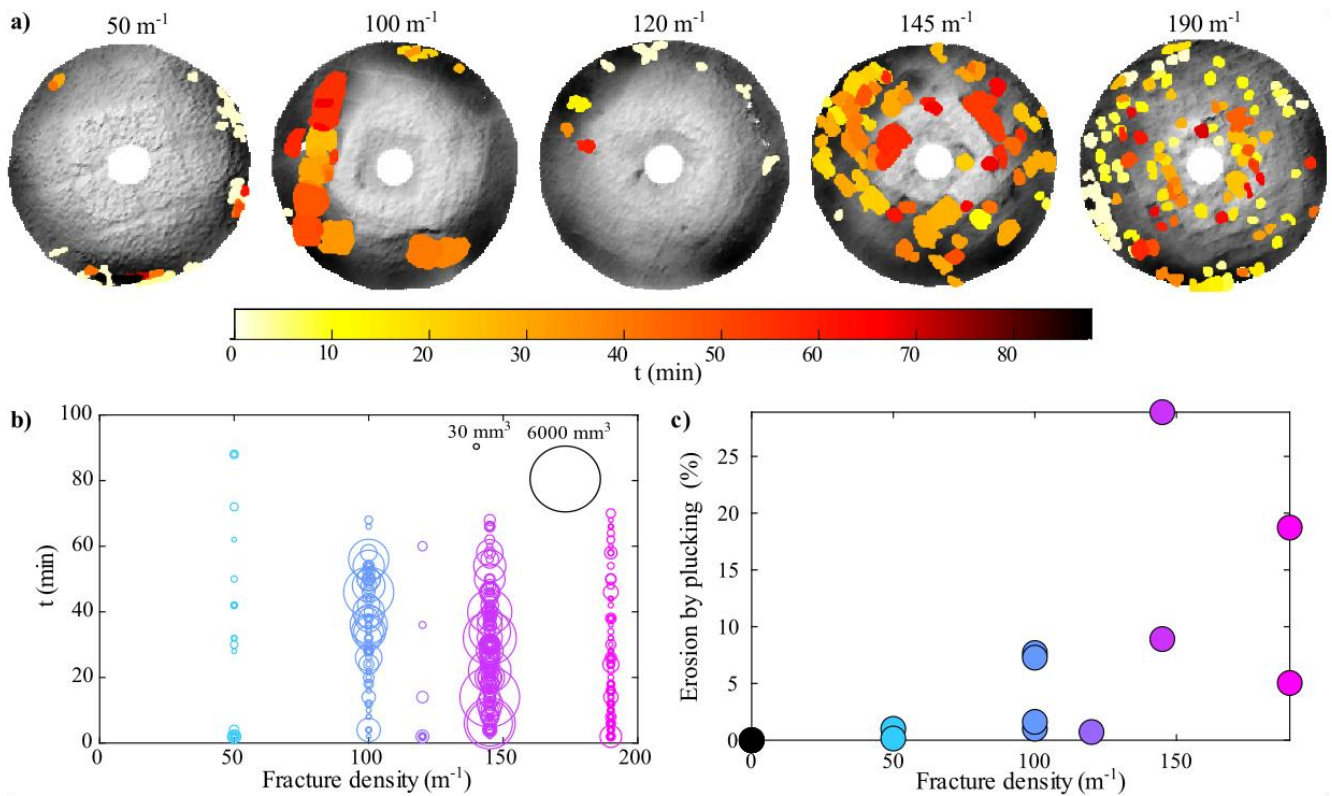


Figure 4: Location, size and time of the detected plucking events for experiments with different fracture densities a) in map view (from 50m-1 to 190m-1 from left to right, the flow direction is clockwise), ad b) as a function of time and fracture density for all experiments with vertical fractures. The size of the circles is proportional to the volume of the plucking event. c) Contribution of plucking to total erosion (in %) with respect to fracture density for experiments with vertical fractures.

similar experiments (Fig. 3c). The deviation. The most notable feature is the larger spreads of average erosion rates for the experiments with fracture density of 100 m^{-1} and 145 m^{-1} show larger spreads and higher average erosion rates (Fig. 3c). However, the range of values is similar to what is observed in other runs so that we do not observe a specific relationship between the fracture density and the average erosion rates (Fig. 3c, Table 1). As fracture density is related to the spacing of the fractures, these experiments show (Fig. 3c). These results show that the spacing of the fractures does not significantly affect the intensity of erosion.

Rather than looking at average erosion of the disk but creates a larger temporal and spatial variability in erosion rates that translates into a larger spread of average erosion rates, we now explore the distributions.

The probability density function of local erosion rates for all the experiments (Fig. 3d). All shows that all runs follow the same trend nearly exponential decrease for local erosion rates of less smaller than 1 mm/min , but. At higher rates, two behaviours emerge at higher rates: the distributions of local erosion for the experiments with no fracture or low fracture density continue to decrease exponentially with about the same trend, while the distributions for experiments with high fracture density deviates and show a heavy-tail distribution (Fig. 3d). Such These high fracture density experiments are the ones prone to plucking (Figs. 2 and 3) and we therefore suggest that the shape of the local erosion rate distribution reflects the occurrence of plucking events (Figs. 2 and 3) showing that the heavy-tail is a signature of plucking. The exponential decay would thus be a signature of abrasion processes. The pdf of local erosion rates shows that plucking events correspond to a maximum of 5.6 mm/min , which is more than half the thickness of the disk eroded between two digitisations (2 min). We note that the local erosion patches observed in the unfractured or low-density fractured experiments (fig. 2b, 2d) have erosion rates that are below the 1 mm/min threshold and do not contribute to the heavy-tail behaviour.

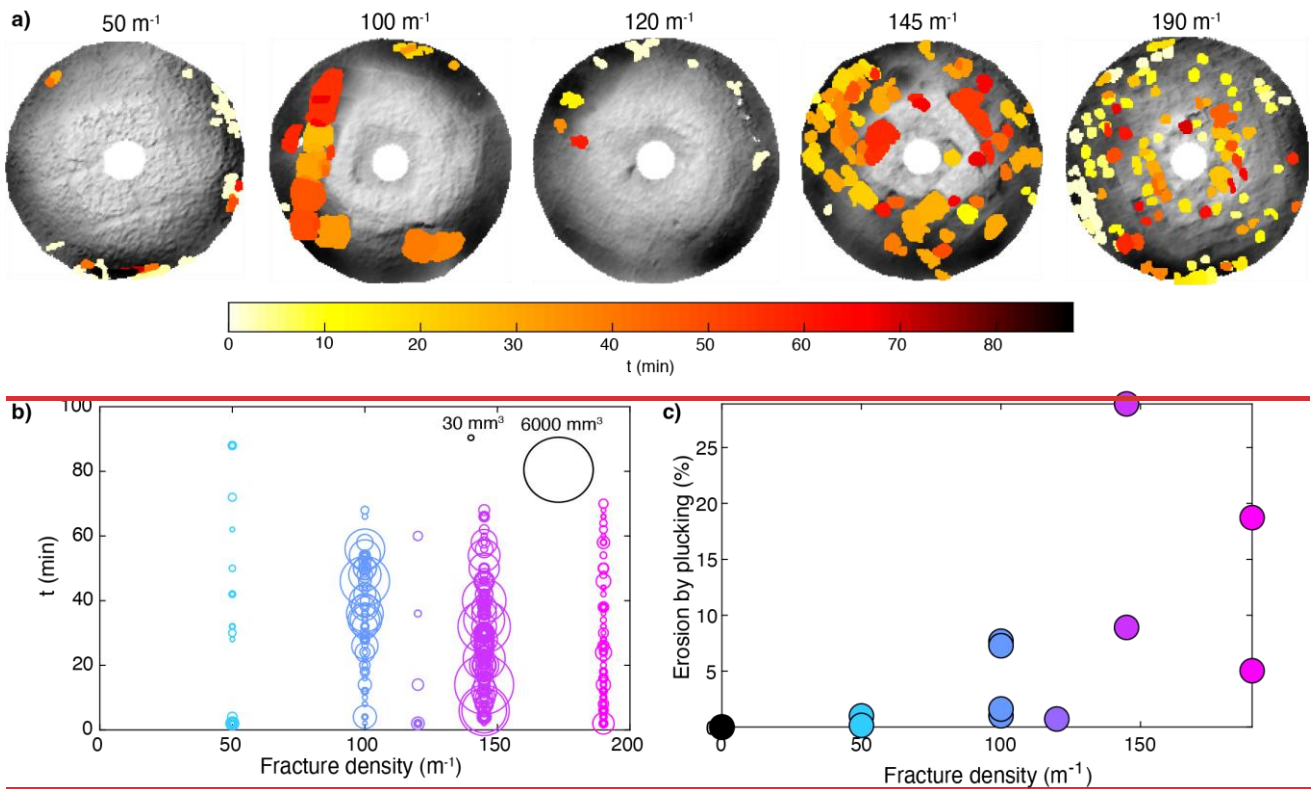


Figure 4: Location, size and time of the detected plucking events for experiments with different fracture densities a) in map view (from 50m⁻¹ to 190m⁻¹ from left to right), ad b) as a function of time and fracture density for all experiments with vertical fractures. The size of the circles is proportional to the volume of the plucking event. c) Contribution of plucking to total erosion (in %) with respect to fracture density for experiments with vertical fractures.

450 **3.3 Occurrence and intensity** 3.3 Influence of fracture density on the frequency, size, and proportion of plucking is controlled by fracture spacing

For all experiments and intervals, we automatically detect the size and the timing of plucking events erosion patches, defined as areas of 15 mm² minimum (based on visual inspection of plucking events from the time series of topographies) with ana minimum erosion rate of minimum 1 mm/min per pixel (based on the change in behaviour change observed above 1 mm/min on in Fig. 3d). As it is not possible to differentiate between one large event or multiple events occurring close to each other during the same time interval, in the following, one plucking event corresponds to the removal of one or several adjacent blocks during the 2 minute time interval. In all experiments, plucking events are observed over the whole duration of the run (Fig. 4a). When the fracture density is low, only a few plucking events located on the edges are observed whereas they tend to occur over the whole surface with higher fracture density (Fig. 4a). In particular, experiments with a very dense network (190 m⁻¹) show numerous small plucking events with 90% of them smaller than 300 mm³ and located all over the surface of the disk (Fig. 4a). The experiment with a fracture density of 120 m⁻¹ behaves as a low density one, and this could be related to the shape of the blocks (see Discussion). The area of the plucked blocks can correspond to the spacing of the fractures but we also document plucking that are smaller or larger than the fracture spacing (Fig. 4a). we define one erosion patch as one plucking event during the 2-minute time interval.

465 Another way to document these patterns is to look at the time of occurrence and volume of events according to the fracture density (Fig. 4b). Plucking can occur at any time during a run and experiments with intermediate fracture density (≥100 and <150 m⁻¹) have a higher tendency to remove large volumes by plucking than the other experiments. The absence of temporal trends (also visible on the full time series of erosion maps in Supplement material, Fig. S5) supports the idea that our disks are quite easy to erode, with blocks already almost detached, as no major period of weakening is required before block removal can occur.

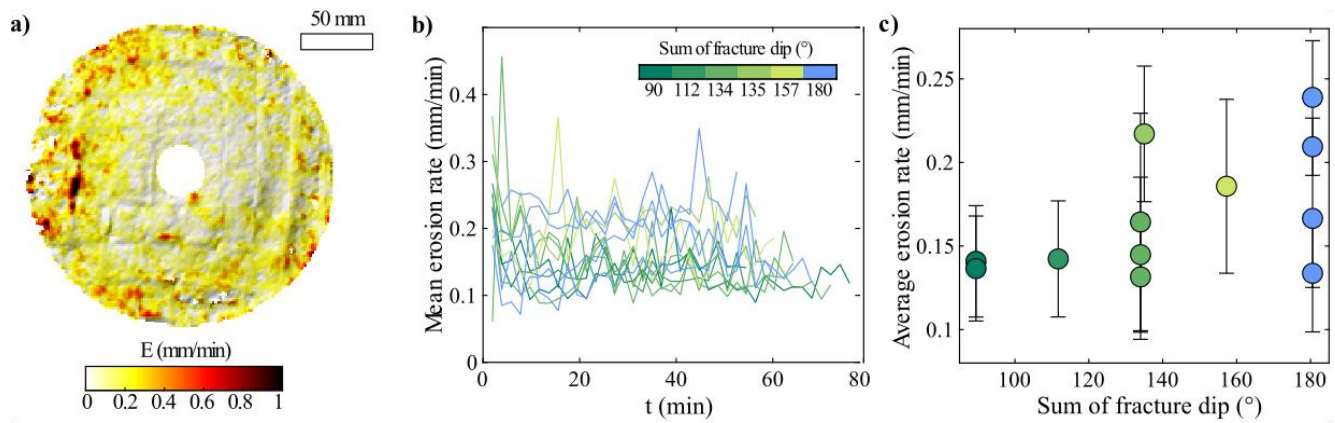


Figure 5: Impact of the fracture dip angle on the average erosion rates with a) an example from a 45/45 ° experiment (the flow direction is clockwise), b) the mean erosion rate with respect to time for the dip angle experiments, and c) the average erosion rate with respect to the sum of fracture dip angles. The bars correspond to the standard deviation, the blue colour corresponds to experiments with vertical fractures (90/90 °), and a spacing of 20/20 mm shown in previous figures

Finally, for each experiment, we calculate the proportion of erosion occurring by plucking with respect to the total erosion of the disk. We observe that the proportion of plucking to total erosion increases with increasing fracture density to a maximum of 29% in experiments with dense fracture network ($p_{21} = 145 \text{ m}^{-1}$) and then seems to decrease for the highest density explored here ($p_{21} = 190 \text{ m}^{-1}$) (Fig. 4c, Table 1). This decrease correlates well with previous observations that plucking events are numerous but not intense in the highest-density network experiments (Fig. 4a-b). This behaviour suggests that plucking is favoured in our experiments with an intermediate fracture density, corresponding to an average fracture spacing of 15–20 mm. Fracture spacing thus exerts a strong control on erosion mode by allowing plucking to occur. However, in the conditions of our experiments, plucking is never the dominant mode of erosion as it accounts for a maximum of 1/3 of the total erosion (Fig. 4c, Table 1). In addition, due to the stochastic behaviour of plucking, experiments with similar fracture networks do not have the same contribution of plucking so we suggest fracture spacing only provides favourable conditions for plucking.

The map views of detected plucking location (Fig. 4a) show that the size and location of these events differ for each fracture density. Experiments with a very dense fracture network (190 m^{-1} , 10/10 mm spacing) exhibit numerous small plucking events scattered across the disc surface. While experiments with a sparse fracture network (50 m^{-1} , 40/40 mm spacing) exhibit only a few small events ($< 50 \text{ mm}^3$) through time. The 120 m^{-1} (10/35 mm spacing) experiment exhibits only a few detected plucking events located on the edges of the disk (Fig. 4a). We observe that for the 100, 145, and 190 m^{-1} experiments, the detected plucking events reflect the shape of the underlying fracture network (Fig. 4a), while the 120 m^{-1} exhibits very few plucking events.

During the experiments, the volume and frequency of detected plucking events vary with the fracture network. Plucking events can occur from the very beginning of the experiments, and there is no clear and systematic increase or decrease in plucking size with time for a given experiment (Fig. 4b). The experiment with a low fracture density (50 m^{-1}) exhibits only a few small events ($< 50 \text{ mm}^3$) through time. The 120 m^{-1} experiment (20/35 mm spacing) behaves similarly to a low-density one. Apart from this, experiments with fracture network densities above 100 m^{-1} (100, 145, and 190 m^{-1}) exhibit more regular plucking events. The 190 m^{-1} experiment shows small volumes (90% of them smaller than 300 mm^3), constrained by the size of the fracture network. While 100 and 145 m^{-1} (respectively 20/20 mm and 10/20 mm spacing between the fractures) exhibit higher volumes, up to 5000 mm^3 .

Apart from the 120 m^{-1} experiment, the contribution of plucking to total erosion tends to increase with the fracture density (Fig. 4c, Table 1). A maximum of 29% is observed for one 145 m^{-1} experiment, showing that plucking events never dominate the total erosion under the studied experimental conditions. As there are large differences in the contribution of plucking to total erosion between experiments at 145 m^{-1} and 190 m^{-1} (from 5 to 29%), we cannot conclude on a specific trend between the percentage of plucking and fracture density above 100 m^{-1} .

3.4 Fracture Influence of fracture orientation and dip with respect to the flow ~~controls the occurrence of plucking~~

In natural environments, fractures are rarely all exposed vertically or normally to the riverbed surface. To further explore the role of fractures on erosion processes, we now focus on the seven ~~Recall that the surface fracture spacing is kept constant at 20 mm in this set of experiments, and that we include in the analysis the previous experiments in which we vary the dip angle of the fractures together with the ones~~ with vertical fractures and 20/20 mm spacing (Table 1). ~~(sum of fracture dip = 180 °).~~

At first order, ~~these experiments~~ with varying fracture dip angles behave like the previous ones: 1) erosion occurs by abrasion and plucking, 2) fractured experiments (fig. 5): (1) erosion rates increase toward the edges (Fig. 5a), and 3) the (2) mean erosion rates range between 0.408 and 0.345 mm/min and converge toward about 0.15 mm/min after 20 minutes (Fig. 5b). However, in details, our experiments show an impact of the fracture dip angle on erosion rates and plucking intensity and location. The)

(3) average erosion rates range between 0.14 ± 0.03 and 0.24 ± 0.03 mm/min and are again associated with large standard deviations (Fig. 5c, Table 1). Yet, we note that experiments with large total dip angles ($>135^\circ$) display average erosion rates more scattered than the ones with low total dip angles ($<135^\circ$) and that the maximum average rates are observed from the higher dip angles (Fig. 5c). Plucking occurs in all runs and at any time during the experiment (Fig. 6a). The volume of (Fig. 5c) and (4) plucking events are observed (Fig. 6). However, experiments with very inclined fracture dip (sum of fracture dip

angles $< 134^\circ$) exhibit specific characteristics: they have a lower mean erosion rate variability and detected plucking events are much smaller and more infrequent than for more vertical fractures (Fig. 6a,b). Consequently, they have a contribution of plucking to total erosion close to zero (Fig. 6c) and behave closer to the vertical fracture experiments with the lowest fracture density (50 m^{-1}).

One combination of fracture dip at 157° ($90^\circ + 67^\circ$) generates a much higher contribution of plucking to total erosion (22 %) than with any other dip combination (Fig. 6c), but also the most pronounced asymmetric pattern of the entire set of experiments (Fig. 6a). We note that asymmetric patterns of plucking are not specific to inclined dip for this fracture spacing (e.g., fig. 4a, experiment 100 m^{-1}), however, it is far more pronounced for this 157° experiment. The area of increased plucking is centred on the zone where the flow is parallel to the vertical fracture and dip in the upflow direction.

While only one experiment is shown in fig. 6, a repeat experiment showed a similar pronounced asymmetry early on, but the experiment was stopped after 16 min due to a runaway entrainment of half of the disk through multiple plucking events (see

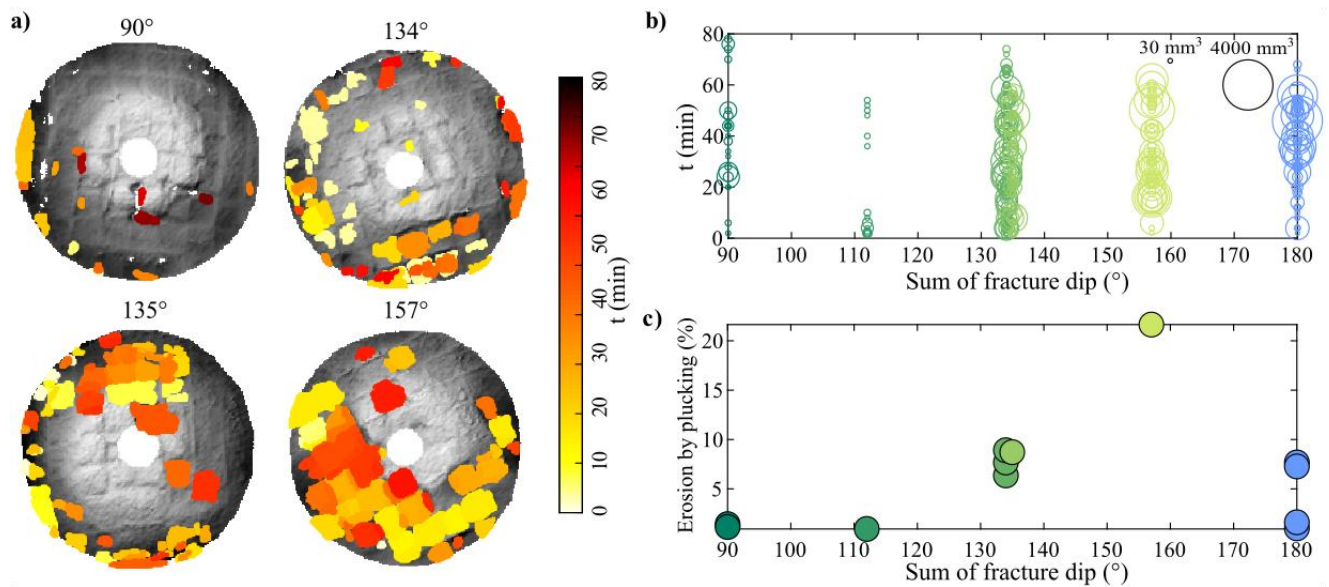


Figure 6: Location, size and time of the detected plucking events for experiments with different fracture dip angles a) in map view (45/45 °, 67/67 °, 90/45 °, 90/67 °; the flow direction is clockwise), and b) as a function of time and fracture density for all the experiments with different dip angles. The size of the circles is proportional to the area of the plucking event. c) Contribution of plucking to total erosion (in %) with respect to the fracture dip angles. The blue colour corresponds to the 90/90 ° network with a 20/20 mm spacing shown in previous figures.

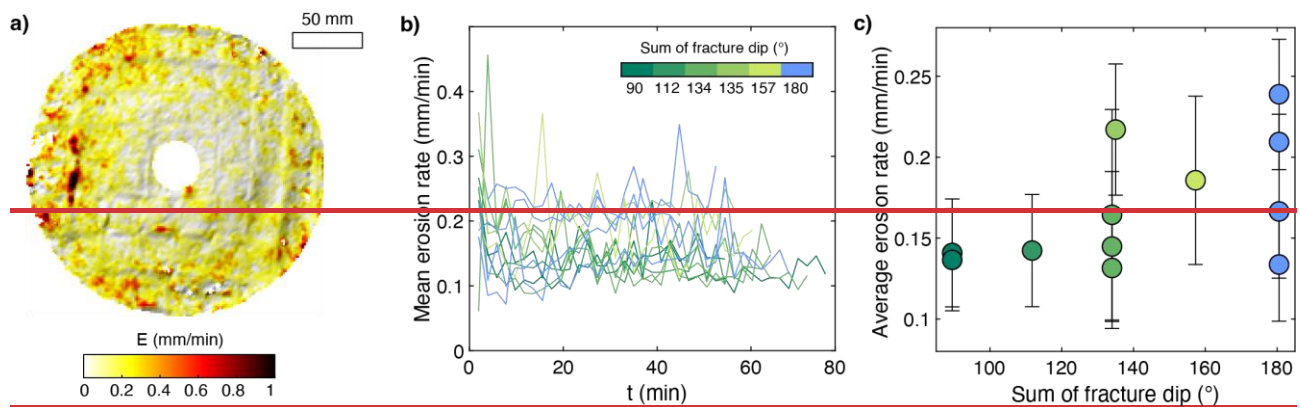


Figure 5: Impact of the fracture dip angle on the average erosion rates with a) an example from a 45/45 ° experiment, b) the mean erosion rate with respect to time for the dip angle experiments, and c) the average erosion rate with respect to the sum of fracture dip angles. The bars correspond to the standard deviation, the blue colour corresponds to experiments with vertical fractures (90/90 °), and a spacing of 20/20 mm shown in previous figures.

supplementary material S7). It is an extreme case of asymmetric plucking showing that the pronounced asymmetry (Fig. 6a) and percentage of erosion by plucking (22 %, Fig. 6c) is not due to a single outlier, but to the specific combination of dips.

3.5 Geometry of plucking events

Combining all fractured experiments, the depth of detected plucking event, d (defined as the plucked blocks is less spread than in the experiments with various spacing (Fig. 4b), supporting the idea that the size of volume divided by the plucked blocks is correlated to the spacing between fractures although we again observe blocks that are smaller or larger than the fracture spacing (Fig. 6a). We note that the size of the plucking events is smaller for the experiments with low total dip angle than for the others (Fig. 6b). This suggests that when fractures are not vertical, it is difficult to remove large volumes by plucking due to the limited depth of a block.

Our results show that the higher the dip angle, the higher the proportion of plucking to total erosion (Fig. 6c). In fact, plucking is quite limited in our experiments with low dip angles (45/45 °, 45/67 °) and its contribution to total erosion is of only a few percent (Fig. 6c). It increases to up to 10 % for intermediate dip angles (67/67 °, 90/45 °) and reach a maximum of 22 % for the 90/67 ° experiment. However, it decreases to less than 10 % when fractures are vertical (90/90 °) (Fig. 6c). We thus observe

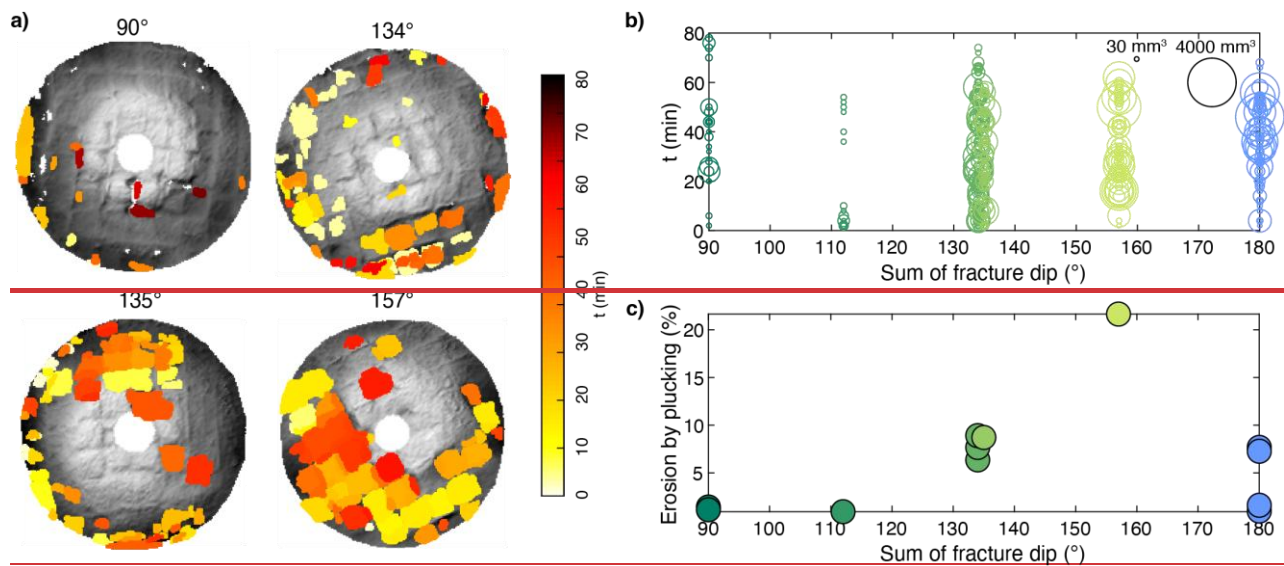


Figure 6: Location, size and time of the detected plucking events for experiments with different fracture dip angles a) in map view (45/45°, 67/67°, 90/45°, 90/67°), and b) as a function of time and fracture density for all the experiments with different dip angles. The size of the circles is proportional to the area of the plucking event. c) Contribution of plucking to total erosion (in %) with respect to the fracture dip angles. The blue colour corresponds to the 90/90° network with a 20/20 mm spacing shown in previous figures.

no clear relationship between the dip angle of fractures and we suggest that the main impact of fracture dip angle is the location of plucking events. In fact, in experiments with non-vertical fractures, we observe a preferential location of plucking events on one side of the disk (Fig. 6a), resulting in a quite asymmetric pattern of erosion in such experiments. On the contrary, plucking events are more spread over the whole surface of the experiments with vertical networks (Fig. 4a) and erosion intensity is more homogeneous.

4 Discussion

In the discussion, we now consider all our experiments together. Our results demonstrate that fractures in bedrock exert an influence on river erosion mode rather than on erosion rates. In fact, the average erosion rates of all our experiments vary within a factor 2 (from 0.13 ± 0.05 to 0.26 ± 0.07 mm/min, Table 1), but we could not identify a clear relationship with network geometry. We observe that the density of fractures controls the occurrence of plucking while the dip angle influences the location of plucking. In addition, the occurrence of plucking influences the location of subsequent plucking events. In consequence, the topography of the disk is controlled by fracture density with a smooth surface when there is no plucking and a sharper one when it occurs. Plucking is never the dominant mode of erosion as even in the most favourable conditions, it accounts for less than 1/3 of the total erosion. Here, we explore some limitations of these results and propose some general interpretations.

4.1 Benefits and limitations of the new experimental setup with fractures

To our knowledge, this study is the first to explicitly integrate fractures geometry in an experiment investigating river bedrock erosion. In contrast to previous experiments where pluckable blocks were pre-existing, our setup requires the third joint to develop in situ during the experiment. This approach allowed us to investigate plucking as an emerging erosion process resulting from likely complex interactions between water flow, grain mobilization and impact, slip along fractures and damage in the concrete disk. To develop this new experiment, we relied on BVOH, a plastic material that dissolves when immersed in hot water, to print the synthetic fracture networks. However, in our setup, plastic dissolution is not fully achieved and softened plastic remains in the fracture plane of width 0.9 ± 0.1 mm. As provided by the supplier, the intact plastic (i.e., before being in

contact with water) has a tensile strength of 45 MPa, which is greater than the one of the concrete (3.01 ± 0.04 MPa). We can assume that the effective tensile strength of the softened plastic is less than its intact value, yet we have no clue whether it is lower than the one of the concrete. In case the tensile strength of the softened plastic is greater than 3.01 ± 0.04 MPa, it could explain 1) why some plastic chunks were protruding from the disk surface in some experiments and 2) more importantly, why disks with fractures tend to erode at lower rates than the disks without fractures during the first 10–20 min (Fig. 3). Indeed, tensile strength is considered as a suitable proxy for rock resistance to abrasion (Sklar and Dietrich, 2001, Turowski et al., 2023), and adding resistant plastic fractures to concrete disks should increase effective tensile strength and hence reduce erosion rates by abrasion.

Moreover, the tensile strength of printed plastics tends to vary with the orientation. For instance, for a very similar plastic material (i.e., natural and not white BVOH), the tensile strength varies between 8.7 and 33.7 MPa, for the ZX (vertical plane) and XY (horizontal plane) orientation. If this information is not known for the white BVOH that we used in our experiment, most printed plastics tend to be anisotropic (e.g., Grant et al., 2021). We therefore suspect that this likely dependency of tensile strength to orientation (i.e., larger tensile strength for fracture planes orientated horizontally than vertically) could partly explain why disks with fractures of limited dip angles have lower erosion rates and proportion of erosion by plucking (Figs. 5 and 6).

The synthetic fracture networks in our experiments also represent end members in terms of fracture size distribution, as most fractures have the same area or length, only varying due to the disk shape. In natural settings, fracture length tends to follow power law distributions with negative exponents (e.g., Bonnet et al., 2001), leading to less frequent long fractures compared to small ones. At the first stage of the study design, we considered printing fracture networks based on more realistic size distributions using for instance a Discrete Fracture Network (DFN) model (e.g., Le Goc et al., 2019). However, our tests with DFN models lead to experimental issues such as isolated volumes which cannot be easily filled up by fresh concrete or isolated fractures requiring numerous mechanical supports during printing.

To characterize the fracture network used in this study, we use the p_{21} as a classic proxy for fracture density and the sum of fracture dips as a proxy for the vertical organization of the fractures. However, these parameters do not fully describe the complexity of the networks as they account for only part of the geometry. For example, they give no information on the shape of the block formed by the fractures (square vs rectangle) or on the asymmetry of the fractures ($45/45^\circ$ vs $90/45^\circ$). Yet it is likely that such complexities play a role on the mode and location of erosion. We explored other parameters such as the average spacing of the fractures or the p_{32} , but we observed no or weak relationships with the average erosion rates or the erosion by plucking. We thus decided to keep the simplest proxies while keeping in mind that they are imperfect.

Therefore, we believe that future work should try to account for a more realistic fracture size distribution and a more accurate (yet simple) description of the fracture geometry to understand how this affects modes of erosion and the size distribution of plucking events.

4.2 Geometry of plucking events

area), tends to increase with area, a , following a power law relationship with an exponent of 0.16 ± 0.03 (Fig. 7a). Our detection of plucking events is based on area and depth thresholds that we defined from visual inspection (area) and from local erosion rates distribution (depth, Fig. 3d) and applied to the difference between two consecutive topographies acquired at 2 min time interval. However, areas affected by plucking might also be eroded by abrasion during the 2 min time interval and areas labelled as abrasion might have experienced small plucking events that are below our thresholds. In both cases, this would lead to a slight overestimation of erosion by either processes that we cannot quantify due to our limits to detect topographic changes (0.2 mm of uncertainties) and temporal resolution (2 min). In addition, these two mechanisms could be considered as a continuum of erosion processes (Beer and Lamb, 2021) so that using a sharp threshold, as we do here, implies that we do not capture this continuum. A single plucking event in this analysis could therefore be the amalgamation of several smaller events

605 occurring next to each other or on top of each other in the 2-minute time interval. The comparison with concrete fragments found in the tank (Fig. S4) supports the possibility of having single plucking events that are several mm thick (Fig. S4). High plucked depths are only observed in experiments with fracture spacing of 20 mm (200 and 400 mm², corresponding to 10 by 20 and 20 by 20 mm, respectively, Fig. 7b). We note that a few of the detected events are larger than the area between fractures for all experiments except for the lowest fracture density (1600 mm²).

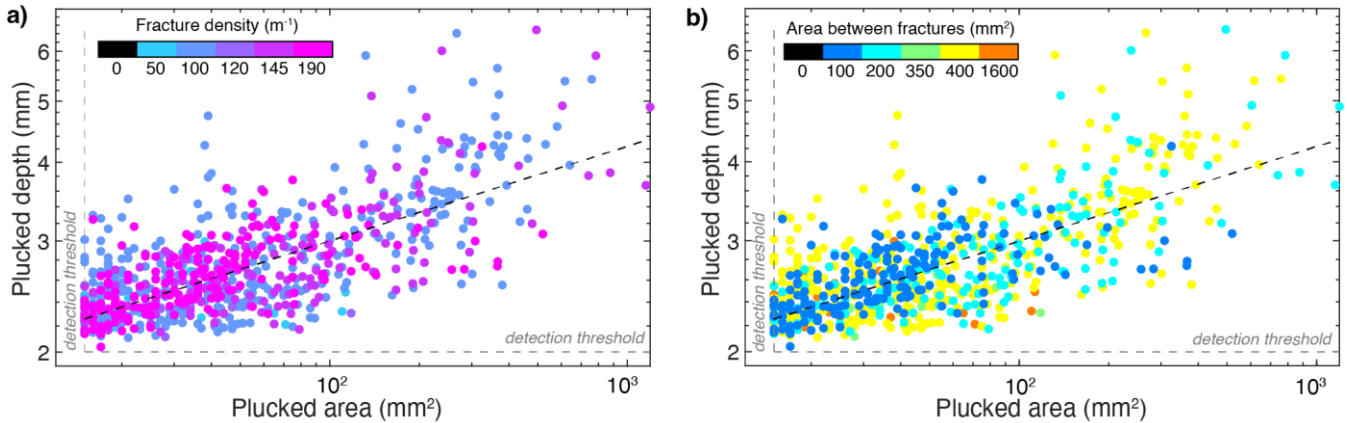


Figure 7: Plucked depth with respect to the plucked area colored as a function of a) the fracture density and b) the area between fractures, for all the experiments. The grey dashed lines indicate the detection thresholds and the black one corresponds to the best fit through the data (see text for details).

610 Keeping in mind these limitations, we now look at the average depth of plucking events, defined as the plucked volume divided by the plucked area. Whatever the fracture density, the depth of plucking event, d , tends to increase with area, a , following a power law relationship (Fig. 7a). We suggest that the relationship between depth and area is related to the mechanical strength of the concrete. When plucking events are small, it is not possible to have small but deep plucking as it is mechanically difficult to dislodge from the surrounding rock mass. When plucking area increases, the depth must increase as well to give the fragment some mechanical strength as large and thin ones are likely to break very easily and to detach as small plucking events. The maximal depth might be limited first by the capacity of the flow to detach concrete fragments and second, by the initial fragmentation of the concrete. In fact, all plucking events have a depth that is only part of the total disk thickness (20 mm), which implies that plucking occurs together with or after the sub-horizontal fracturing of the concrete. In experiments affected by plucking, we do not observe a time lag in the occurrence of plucking (i.e., plucking occurs from the very beginning on the run, Figs. 4b and 6b). This suggests either 1) that the concrete is already partially fractured before the experiments start, which could result from the contraction occurring during the hardening phase, or 2) that concrete fracturing occurs rapidly under the action of water flow and sediment impacts during the experiment, due to its low tensile strength. We note that when a plucking event is detected, we are not able to differentiate between one single event or an amalgamation of several smaller events occurring next to each other or on the top of each other in the 2-min time interval. For example, the large depths of 6 mm could simply be the removal of two 3 mm thick blocks at the same location. However, some of the concrete fragments we found when we emptied the column to photograph its surface are several mm thick (Fig. S3) supporting the idea that both mechanisms (unique or amalgamated event) are likely to occur in our experiments. The area of the initial blocks defined by the fracture network does not control the area of plucking events as we observe plucking events of any size in almost all experiments (Fig. 7b). However, high plucked depths are only observed in experiments with fracture spacing of 20 mm (200 and 400 mm², corresponding to 10 by 20 and 20 by 20 mm, respectively). This suggests once again that this spacing is optimal to plucking. We note that it corresponds to the average size of the impactors used in this study (our gravels are 1–2 cm in diameter), but we would need dedicated experiments to further investigate this point.

625

630

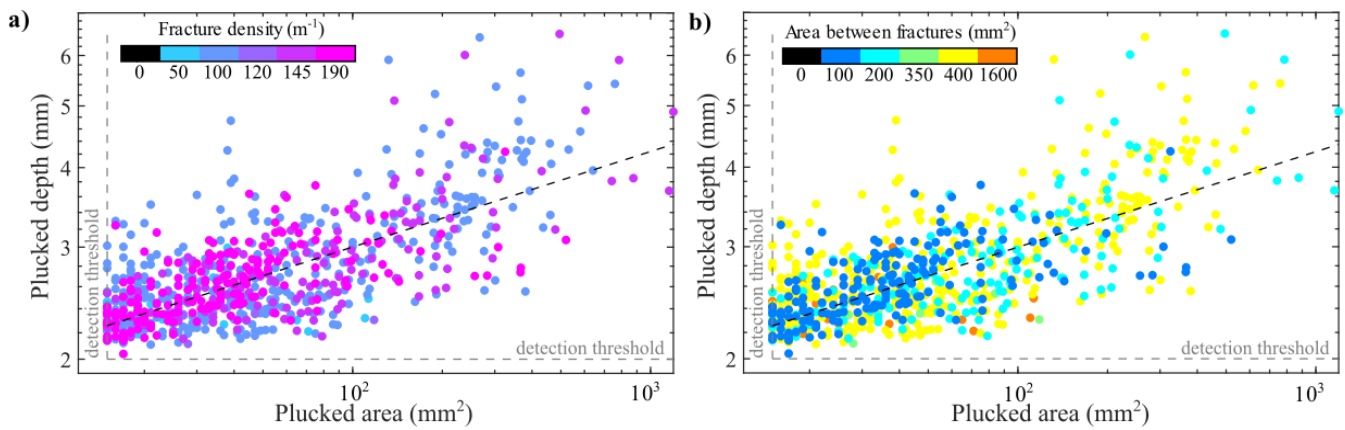


Figure 7: Plucked depth with respect to the plucked area coloured as a function of a) the fracture density and b) the area between fractures, for all the experiments. The grey dashed lines indicate the detection thresholds and the black one corresponds to the best fit through the data (see text for details).

4.3 Plucking and spatial patterns of erosion

In the previous sections, we show that there is no clear relationship between the geometry of the fracture network (characterized either by the fracture density or by the total dip) and the average erosion rates (Figs. 3c and 5c). However, we observe a control of the fracture network on the occurrence of plucking, both in terms of plucking location (Figs. 4a and 6a) and of contribution to total erosion (Figs. 4c and 6c). In experiments with non-vertical fractures, we observe that plucking tends to be located on one side of the disks, inducing more intense local erosion (Fig. 6a). We suggest that this dissymmetric spatial distribution relates to the orientation of the fractures with respect to the flow. Once plucking has been initiated, where the fractures face the flow (lower part of the bottom right disk on Fig. 6c for example), the local relief is sharper, which in turn promotes plucking. On the contrary, when the fractures are aligned with the flow (upper part of the bottom right disk on Fig. 6a), the local relief is smoother and impacts are less efficient, promoting abrasion. The tendency to pluck might thus not be directly related to the dip angle of the fractures but rather to interactions between the grains and the fractures that have the potential to deviate the grains and to absorb part of the impact energy of the grains.

In an attempt to summarize all our observations, we now 3.6 Plucking and spatial patterns of erosion

Here, we group the experiments according to the contribution of plucking to the total erosion of the disk after 40 min (Table 1), whatever the geometry of the fracture network. Four groups emerge with no plucking (0 % of total erosion by plucking), corresponding to unfractured experiments, low plucking (<5 %), limited plucking (>5 % and <10 %), and high plucking (>10 %). We calculated Fig. 8a shows that the average erosion rate of each group, and we observed that it increases with the increasing erosion by percentage of plucking (Fig. 8a). In fact, the average erosion rate is close to 0.17 mm/min with no plucking and reaches up to 0.21 mm/min with high plucking. In line with the results presented here, we note that the lowest rate (0.15 mm/min) is observed for fractured experiments with low plucking (light blue in Fig. 8a) rather than for the unfractured experiments with no plucking (dark blue in Fig. 8a).

To better understand this behaviour, we now look at the spatialization of erosion along the disks. For each experiment, we extract the radial profile of total erosion according to the distance from the centre of the disk after 40 minutes of erosion (Supplement 45, Fig. S4S5). The profiles show quite large scatter and therefore, for each run, we determine the mean erosion profile, and for each group, we calculate the average cumulated erosion (Supplement 45, Fig. S4S5). In experiments with no fractures and plucking (dark blue, Fig. 8b), there is almost no erosion between 0 and 30 mm away from the centre of the disks. Erosion then increases with distance to about 70 mm before decreasing slightly toward the edges of the disk. These experiments with no plucking have the highest total erosion in the distal parts of the disk (distance >55 mm, Fig. 8b). For fractured experiments with low or limited plucking (light blue and orange, Fig.

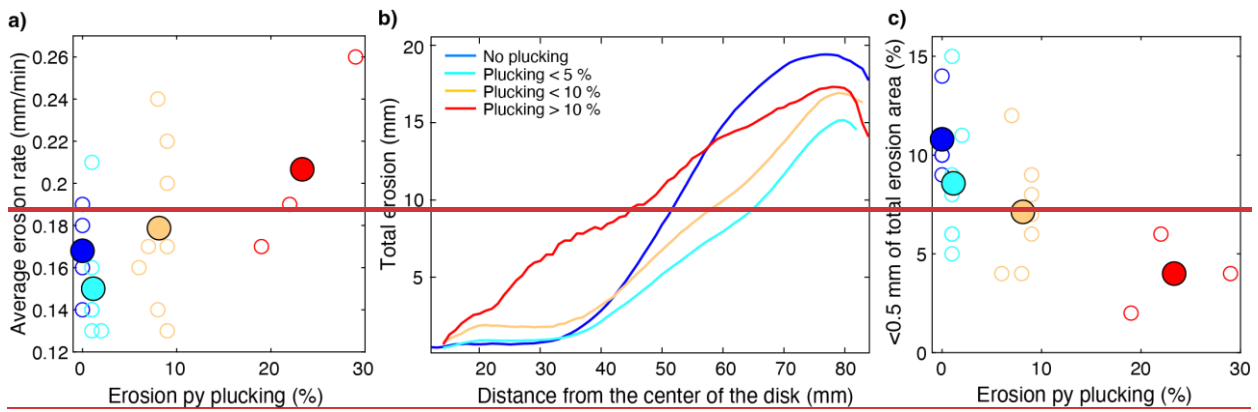


Figure 8: Impact of the erosion by plucking on a) the average erosion rate, b) the total erosion after 40 min of run and according to the distance from the centre of the disk, and c) the area with limited total erosion, for all the experiments presented in this study grouped by their percentage of erosion by plucking (group 1, dark blue: no plucking, group 2, light blue: plucking <5 %, group 3, orange: plucking <10 % and group 4, red: plucking >10 %). On panels a and c, white dots are for individual runs, coloured dots are for the average of the group. On panel b, only the average curves are shown.

8b), erosion is also very limited from 0 to 30 mm away from the centre of the disk and then increases radially, but slowly than for the previous group: unfractured experiments. Experiments with high plucking (red, Fig. 8b) have a similar evolution maximum total erosion in the most distal part of the disks (>40 mm from the centre) where the cumulated erosion increases continuously toward the edges. However, these experiments show disk, but they exhibit a different pattern: lower asymmetry along the radial profile, with a significant amount of erosion in the proximal part of the disk (between 0 and 40 mm) around 20 mm from the centre of the disk. 50 mm. Therefore, the main impact of when plucking seems to be the growth of becomes significant, it extends the area submitted to erosion, extending towards the centre of the disk. To support this idea, for each group, we calculated the area that was only slightly eroded (defined as a pixel with less than 0.5 mm of total erosion over the whole duration of the experiment, based on the erosion profiles of Fig. 8b). We indeed observe that the 8b. The proportion of low erosion areas decreases from about 11 % for to 4% with the proportion of erosion by plucking (Fig. 8c).

In other words, the presence of fractures in the disks modifies the shape of the erosion profile and the location of plucking events, leading to a counter-intuitive decrease in total erosion in experiments with low plucking and a limited increase for other experiments. The change in the spatial pattern of erosion seems to be the main control on the average erosion rates and suggests that plucking does not increase the erosion intensity itself, but rather extends the area submitted to erosion. Although plucking occurs from the very beginning of a run (Figs. 4b and 6b), the location of plucking tends to evolve through time as it is first mostly located on the edges of the disks before to progress toward the centre of the disks (Fig. 2). As more area is eroded, the total erosion increases. This suggests that the main influence of fractures, whatever their geometry, is either to absorb the impact energy or to deviate the grains so that there are fewer impacts on the edges of the disks, therefore less intense erosion but slightly more in the middle. This is beyond the scope of the present study to investigate these processes further.

680 4.4 Integration of our experiments with previous studies on plucking

In our erosion mill, we investigate the erosion dynamics of fractured concrete disks through both abrasion and plucking. While abrasion has already been studied using similar setups (Sklar and Dietrich, 2001; Turowski et al., 2023b), this is the first study to incorporate the process of plucking within this setup. Previous studies on plucking were conducted in flume setups with already detached blocks, and focused on the hydraulic forces involved (Wilkinson et al., 2018; Saha et al., 2021; Dubinski and Wohl, 2013). Plaster blocks with no specific shape (Wilkinson et al., 2018) and cubic blocks made of composite material (mix of concrete, sand, Poraver expanded glass and water) with varying density (Saha et al., 2021) were used in setups without any initial bed protrusion. Dubinski and Wohl (2013) used concrete with regularly spaced vertical and horizontal fractures over riverbeds with a pre-existing knickpoint. Results of these experiments demonstrate that plucking can occur even without initial bed protrusion, driven by unsteady, nonuniform flows and local turbulence induced by varying slope and inlet steps (Wilkinson

690 et al., 2018; Saha et al., 2021). Additionally, knickpoints and artificial upstream steps (either imposed by the setup or formed during a run), along with increased bed slope, promote the development of hydraulic jumps and turbulent flow structures, which can significantly enhance block removal processes (Dubinski and Wohl, 2013; Wilkinson et al., 2018). Yet, Wilkinson et al. (2018) observe that local flow may either amplify or limit plucking by altering flow conditions. Moreover, past plucking events lead to new steps and holes, which in turn induce new hydraulic jumps and free surface undulations, which can alter hydraulic conditions and thus the location and dynamics of future plucking events.

695 These studies have constrained the hydraulic processes driving plucking but not the role of bedload impacts, which can contribute to block pre-detachment and influence or even trigger plucking. In our experiments, we encompass both the formation of blocks, as our bedrock consists of a cohesive material with mechanical discontinuities instead of already detached blocks, and their hydraulic entrainment. The discontinuities act as fractures that may define the lateral edges of pluckable blocks, while the bottom face of each block is formed in situ by the damage and fracturing induced by sediment impact. The hydraulic conditions alone may not be sufficient to induce plucking in our experiments, and sediment impacts are likely necessary to form pluckable blocks. Once formed, blocks can be entrained by hydraulic forces or sediment impacts, which may trigger the final lift. Because our blocks are not pre-detached, the potential role of water infiltration in fracture and hydraulic overpressure documented in the field and in other experiments (e.g., Wilkinson et al., 2018) may not play a dominant role in our setup. In terms of results, the main difference between previous hydraulic experiments and our study may lie in the propagation direction of plucking. While earlier studies mainly observe upstream propagation (Wilkinson et al., 2018; Saha et al., 2021; Dubinski and Wohl, 2013), our experiments reveal both upstream and downstream plucking propagation. We hypothesize that this difference in plucking propagation is linked to the role of sediment grain impacts together with flow variability. Once a first block is dislodged, sediments can impact the upstream face of the downstream block, potentially delivering enough energy to entrain it.

700 Then, in contrast with previous studies in which the size of the plucked blocks is fully imposed, the shape of the plucked blocks in our experiments does not always correspond to those of the fracture delimited blocks and the depth of the blocks is an emergent feature in our experiments. In fact, sediment impact can damage and fracture the bedrock both in surface and at depth. This is favoured by the mechanical strength of the fracture network which remains likely significant relative to the one of the concrete. Using these new formed fractures, following impacts can sometimes dislodge only part of the initially delimited block, or, conversely, cause the simultaneous removal of neighbouring blocks still connected along joint surfaces. The depth of plucked blocks tends to increase with their surface area (Fig. 7). This relationship is thought to be controlled by the mechanical strength of the concrete fragments together with the fracture spacing, with maximum plucking depths limited by the sediments and flow effectiveness in material removal, and the geometry of the initial fracture network. Because the shape of the blocks is not always the same, it is likely that, compared to previous work, our setup favours topographic variability and thus, variable flow conditions. This could explain for example why we observe plucking propagation either upstream or downstream.

4.5 From laboratory experiments to natural river

725 While experimental studies provide valuable insights, they necessarily rely on simplified conditions and cannot fully replicate the complexity of natural processes driving plucking. Our experimental setup simplifies several aspects of natural systems to isolate specific erosion processes. Unlike natural bedrock rivers, our experiments use a constant sediment input, identical hydraulic conditions throughout the run, uniform grain size, and a highly erodible substrate. In addition, and similarly to previous experiments, we cannot simulate the full variety of processes that may contribute to plucking in natural settings. For example, in our experimental setup, wedging, i.e., the ability of sediment to lodge themselves between fractures, cannot occur due to the large size of the grains we use with respect to the fracture aperture. Moreover, because our fractures are filled with plastic material, water infiltration is prevented or limited so that we do not expect significant hydraulic pressure fluctuations

inside the fractures. Both factors contribute significantly to plucking under natural conditions (Whipple et al., 2000b), suggesting that plucking may be more efficient in natural settings than in our experiments. In our experiments, plucking leads to locally enhanced erosion where blocks are removed. However, when averaged over the entire eroded surface of the disk, the mean erosion rate does not significantly differ from runs without plucking. This suggests that while plucking creates spatial heterogeneity in erosion, it does not increase overall erosion efficiency at the scale of our experimental setup. This could be partly explained by the relative strength of the plastic fractures compared to the concrete. The result that plucking does not alter erosion efficiency is also consistent with the idea that, in natural settings, plucking may induce transient variations in erosion rates, but rivers eventually adjust their morphology (e.g., slope, width) to maintain a steady-state balance with tectonic uplift.

Yet, we observe similarities between our studies and different field works on river erosion. For example, observations demonstrate that fracture characteristics exert a key control on erosion dynamics in river channels (Chatanantavet and Parker, 2009; Dubinski and Wohl, 2013; Scott and Wohl, 2018; Whipple et al., 2000a). Channels composed of massive bedrock are predominantly eroded by abrasion, whereas those with a dense fracture network are more prone to plucking (Whipple et al., 2000b, Scott and Wohl, 2018). A study by Lima et al. (2021) in the Paraná Basin, Brazil, highlighted the influence of variability in fracture density, type, and orientation at the channel scale on riverbed erosion and morphology. They observed that faults, oriented obliquely to the flow, control the main erosion axes, forming an average relative angle of $\sim 50^\circ$ with the flow direction. Moreover, Lima et al. (2021) observe an increase in plucking intensity (and a decrease in macroabrasion) with fracture density. Our results are consistent with such observations as fracture density favours plucking (Fig. 4c).

The presence of fractures also affects the spatial distribution of erosion. Several studies have shown that more densely fractured rocks exhibit wider valleys (Ehlen and Wohl, 2002; Scott and Wohl, 2018; Snyder et al., 2003; Wohl, 2008). For instance, Carr et al. (2023) documented variations in channel width along a 600 m river section (with a constant grain size distribution) characterized by alternating lithologies of marble and blackschist, with the latter assumed to have a higher fracture density. The blackschist river segment is characterized by a wider valley, up to 120 m, than the marble segment, limited to a width of ~ 70 m. In our experiments, we observe that lower fracture densities lead to narrower spatial distributions of erosion on our disk compared to higher fracture densities (see Fig. 2 c and e). Based on our results, we suggest that the difference in valley width documented by Carr et al., (2023) may result from the difference in fracture density, due its impact on erosion localization.

In addition to its impact on large scale topography, fracture density, via the dominance of abrasion or plucking, can induce a significant roughness of the riverbed. When plucking occurs, roughness increases due to the abrupt changes in the topography after block removal. These changes may create sharp steps or depressions in the surface, often aligned with the pre-existing fractures and the in-situ formed fractures (Whipple et al., 2000b; Fig. 2e). These features contrast with the smoother and more continuous surfaces produced by abrasion (Whipple et al., 2000b; Fig. 2a). Increased roughness enhances flow resistance and promotes small scale turbulence, which can alter local hydraulics and sediment paths in ways that can reinforce block detachment (Whipple et al., 2000b; Wilkinson et al., 2018). Following Wilkinson et al. (2018), this may sustain a feedback loop that promotes plucking. This also suggests that roughness may provide useful insights into the spatial distribution of erosion processes in bedrock rivers.

5 Conclusions

In this study, we developed dedicated experiments of fractured concrete disk erosion to investigate how the geometry of fractures in river bedrock can affect the magnitude, the location and the mode of erosion, by abrasion or plucking. We use temporal series of 3D topographies to document erosion rates and patterns through time.

We show that when there is no fracture, the disks erode by abrasion only and show a smooth topography with a radial symmetry. On the contrary, when the disk is fractured, erosion can occur both by abrasion and plucking, leading to a rougher topography and less radial symmetry. However, we observe no clear relationship between the average erosion rates and the fracture density or dip angle. This is partly because detected plucking never accounts for more than 1/3 of the total erosion in our experiments, and because fracture mechanical strength is likely close to the one of the concrete in our experiments.

Rather than a direct impact on erosion rates, we suggest that the presence of fractures is a required condition for plucking to occur so that the first impact of fractures is on the morphology of the riverbed. Our experimental results show that plucking is favoured by intermediate fracture density (145 m^{-1}), and by intermediate dip angle (67°) which forms blocks that are thick enough to be plucked more easily than with vertical fractures. In addition, we demonstrate that the orientation of the fractures with respect to the flow plays a major role in enhancing plucking, which is favored when fractures dip upstream (i.e., against the flow direction). Finally, we show that plucking alters the spatial distribution of erosion, thereby increasing the overall surface area subject to erosion. Therefore, we suggest that fracture density and dip angle, which can favour the occurrence of plucking, impact riverbed evolution by changing the mode and thus the location of erosion, rather than by promoting greater erosion rates.

This study highlights the need to consider the geometry of fractures in bedrock rivers to fully describe, understand and simulate erosion in rivers and channel evolution through space and time. To support the systematic integration of fractures in future works, the framework developed by Eppes et al. (2024) should be applied to characterize fracture density, shape, and dip in bedrock rivers, so that fracture geometry may become a standard measurement in fluvial studies. Lastly, in line with previous works (Turowski et al. 2023b), the size of sediments with respect to the fracture geometry is likely a key parameter that we intent to further investigate with our experimental setup.

n	Spacing (mm)	Density (m^{-1})	Dip angle ($^\circ$)	Sum of dip angle ($^\circ$)	Mean erosion rate (mm/min)	Standard deviation (mm/min)	Erosion by plucking (%)
1	-	0	-	-	0.18	0.05	0
2					0.19	0.06	0
3					0.16	0.04	0
4					0.17	0.05	0
5	40/40	50	90/90	180	0.16	0.04	1
6					0.14	0.03	1
7	20/20	100	90/90	180	0.24	0.03	8
8					0.21	0.02	1
9					0.17	0.04	7
10					0.13	0.03	2
11			45/45	90	0.14	0.03	1
12					0.14	0.03	1
13			45/67	112	0.14	0.03	1
14			67/67	134	0.16	0.06	6
15					0.14	0.05	8
16					0.13	0.04	9
17			90/45	135	0.22	0.04	9
18			90/67	157	0.19	0.05	22
19	10/35	120	90/90	180	0.13	0.05	1
20	10/20	145	90/90	180	0.17	0.05	9
21					0.26	0.07	29
22	10/10	190	90/90	180	0.20	0.08	9
23					0.17	0.04	19

Table 1: Geometric properties, mean erosion rates with standard deviations and percentage of erosion by plucking for all the experiments. The colours to the right of density and sum of dip angle are the ones used in the figures.

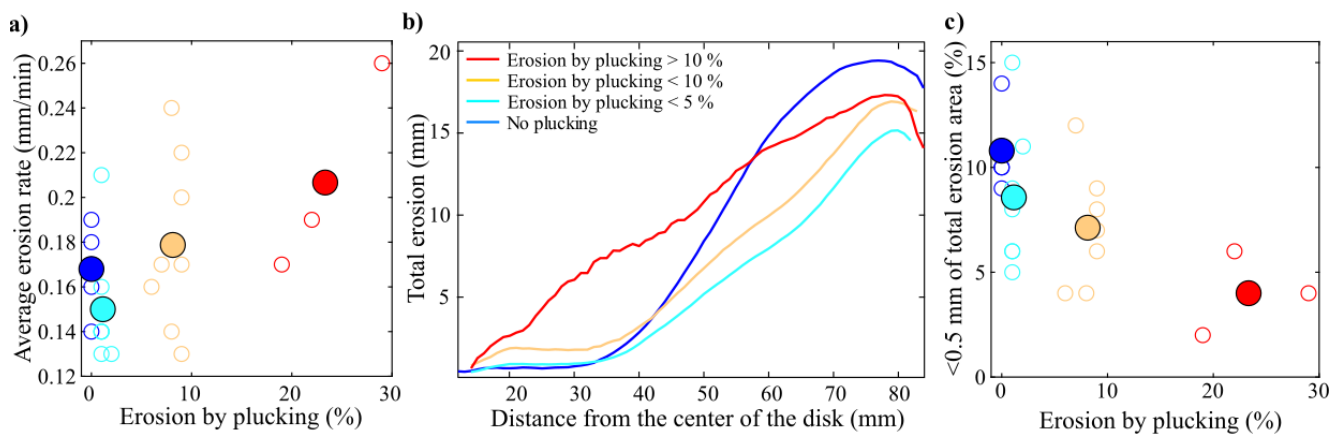


Figure 8: Impact of the erosion by plucking on a) the average erosion rate, b) the total erosion after 40 min of run and according to the distance from the centre of the disk, and c) the area with limited total erosion, for all the experiments presented in this study grouped by their percentage of erosion by plucking (group 1, dark blue: no plucking, group 2, light blue: plucking < 5 %, group 3, orange: plucking < 10 % and group 4, red: plucking > 10 %). On panels a and c, white dots are for individual runs, coloured dots are for the average of the group. On panel b, only the average curves are shown.

4 Discussion

4.1 Benefits and limitations of the new artificial fractured bedrock

795 To our knowledge, this study is the first to explicitly integrate fracture geometry (2D spacing and dip angles) in an experimental investigation of bedrock river erosion with bedload transport. The erosion mill set up we derive from Sklar and Dietrich (2001) and others (Scheingross et al., 2014; Small et al., 2015; Turowski et al., 2023) has the advantage of being compact, easy to set up compared to annular (Attal et al., 2006) or linear flumes (e.g., Wilkinson et al., 2018), and can reach high flow velocities required to transport cm-size gravels. However, it is not designed to reproduce a channel cross-section or river reach as it has a well-known limitation: the strong radial gradient in flow velocity. The resulting centrifugal force drives the grains toward the disk edge, where the flow velocity and shear stress are higher. Consequently, grain impacts are more frequent and more energetic in this part of the disk. A significant difference with previous setups is that our maximum of abrasion is near the mill edge, while in Sklar and Dietrich (2001) and Small et al. (2015), a vertical recirculation prevents grains to reach the mill edge, and the maximum erosion is located several centimetres away from the edge (e.g., about 50 mm in Small et al., 2015). We believe our configuration and the new propeller we used yields saltation trajectories that are less or not affected by vertical recirculation, and thus potentially closer to reproducing small-scale interactions of sediments with the bedrock floor of an actively incising river. In this setup, our main contribution is the development of a new artificial bedrock material with 3D-printed mechanical discontinuities of chosen orientation and spacing. This allows for reproducible heterogeneity patterns and good control on the spatial density of mechanical discontinuities, a parameter that is expected to strongly control erosion efficiency.

810 After several tests of 3D printing material, we chose BVOH to print the synthetic fracture networks, a plastic material that fully dissolves when immersed in hot water. However, in our setup, the cement alters the chemical properties of BVOH and it does not dissolve, but is turned into a softened plastic remaining in the fracture plane of width 0.9 ± 0.1 mm. Consequently, water cannot flow through the fractures, and the blocks are not fully loose laterally. Although the tensile strength of intact BVOH is high and generally depends on orientation, ranging from 8.7 to 33.7 MPa for ZX (vertical) and XY (horizontal) planes, it is strongly reduced in the condition of our experiments. For instance, when the fractured disks are immersed in the column, they cannot be extracted again as they break instantaneously along the fracture planes. However, we note that their softness can create a coating on the fracture planes when they are exposed, which could dampen bedload impacts before being

820 fully abraded. Also, because fractures are filled, water flow and small grains cannot occur in fractures, such that hydraulic
lifting through pressure fluctuations (Whipple et al., 2000b) and wedging by grains (e.g., Hartshorn et al., 2002) cannot occur.
The synthetic fracture networks in our experiments represent end-members in terms of fracture size distribution, as most
fractures have the same area or length, only varying due to the disk shape. In natural settings, fracture length tends to follow
power-law distributions with negative exponents (e.g., Bonnet et al., 2001), leading to less frequent long fractures compared
825 to small ones. At the first stage of the study design, we considered printing fracture networks based on more realistic size
distributions using, for instance, a Discrete Fracture Network (DFN) model (e.g., Le Goc et al., 2019). However, our tests with
DFN models have led to experimental issues, such as isolated volumes that cannot be easily filled with fresh concrete or
isolated fractures that require numerous mechanical supports during printing. For the same reasons, it is not possible to create
a fully 3D fracture network, including horizontal fractures at various depths to create fully bounded blocks.

830 To characterize the fracture network used in this study, we use the p_{21} as a classic proxy for fracture density and the sum of
fracture dips as a proxy for the vertical organization of the fractures. However, these parameters do not fully describe the
complexity of the networks as they account for only part of the geometry. For example, they give no information on the shape
of the block formed by the fractures (square vs rectangle) or on the asymmetry of the fractures ($45/45^\circ$ vs $90/45^\circ$). Yet it is
likely that such complexities play a role in the mode and location of erosion. We explored other parameters such as the average
spacing of the fractures or the p_{32} , but we did not observe clearer relationships with the average erosion rates or the percentage
835 of erosion by plucking.

The setup allowed for very good repositioning of the experiments for 3D scanning and thus provides a detailed 4D record of
the disk evolution. The SFM approach provides accurate topographic reconstruction, yet the very close viewing points of the
4 cameras is not optimal for SFM and point cloud cleaning using Canupo (Brodu and Lague, 2012) was required to remove
reconstruction errors.

840 **4.2 Erosion processes in the experiments: empirical and physical analysis**

Throughout the description of our results, we have referred to two main modes of erosion, abrasion and plucking. We here
discuss the relevance of these processes and the associated definitions in the light of empirical and physical analysis.

Empirically, two modes of erosion emerge in our experiments: 1) a “background” mode characterized by an exponential decay
of the distribution of local erosion rates with limited or no clear spatial clustering of erosion rates, and 2) a “patch” mode
845 leading to a heavy-tailed distribution of local erosion rates and to spatially clustered patches of high erosion rates (Fig. 2 and
3d). We have, for the sake of simplicity, referred to these two modes as abrasion and plucking, respectively, and delimited
them by considering that plucking events correspond to continuous patches of area greater than 15 mm^2 associated with an
erosion rate greater than 1 mm/min . These thresholds are likely related to the scale and conditions of our experiments, to the
accuracy and resolution of the SFM topographic reconstruction, and to the method and time intervals used to differentiate
850 erosion rates. In turn, this binary vision of erosion processes and the associated definitions of plucking and abrasion are intrinsic
to our study and does not rely on a universally accepted definition or delimitation of these processes, as presented in the
introduction.

Physically, our overall results also indicate at least two distinct modes of erosion: progressive wear by impacting particles and
erosion by first block formation and loosening, followed by entrainment. An important feature of this second mode is that the
855 size of the removed blocks does not always correspond to the maximum dimensions defined by the fracture network and the
bottom of the disk. More precisely, the horizontal areal extent of the removed blocks shows a large distribution (Fig. 7), with
a significant proportion of blocks reaching fracture spacing (Fig. 4a). For the vertical dimension, very few blocks erode down
to the bottom of the disk (at a depth of 2 cm), and this occurs only after significant cumulated erosion, reducing the distance
between the disc surface and bottom. The depth of the removed blocks tends to scale with their surface area along a large
860 continuum of size, only generally bounded by fracture horizontal spacing. Overall, this highlights the existence of two separate

865 stages: 1) a fracturing phase, consisting of systematic horizontal fracturing and sometimes vertical fracturing, in which blocks are formed but not necessarily transported immediately, and 2) an entrainment phase, during which detached blocks are removed. The time interval between fracture formation and block removal, as well as the processes leading to fracturing (e.g., sediment impact, coalescence of pre-existing weaknesses) and block removal (e.g., hydraulic transport, sediment impact) cannot be determined. Yet, sediment impact likely plays a significant role, at least for the fracturing phase, as water flow itself does not lead to erosion. In the following, we aim at refining the nature and definition of this process, and whether it corresponds to a unique process or two separate depending on the size of the debris produced with respect to the pre-existing fracture geometry.

870 Horizontal cracks developing between existing vertical fractures due to bedload impacts correspond to the exact plucking process depicted in Figure 4 in Whipple et al (2000b) and Figure 4A in Whipple et al (2022). We thus consider that plucking operates in our experiments and is influenced by fracture spacing and dip (Fig. 4 and Fig. 6). However, the existence of erosion patches smaller than the area between fracture spacing implies that a more complex fracture pattern with vertical and horizontal components can developed at a smaller scale. This is more akin to the definition of macroabrasion occurring in our experiment, either through one large bedload impact removing a large chunk of rock (Beer and Lamb, 2021; Scott and Wohl, 2019) or
875 progressive fracturing in the vicinity of fractures followed by entrainment (Chatanantavet and Parker, 2009). Because high erosion patches are not detected in unfractured experiments, either macroabrasion does not occur, or operates at a level which we cannot distinguish from classical wear. This means that significant macroabrasion exists in our experiments, but only in relation to fractures, exploiting the local mechanical weakness, not as a purely random process. Hence, this structurally driven macroabrasion is likely the process generating cm-scale erosion patches detected near fractures for the largest fracture spacing
880 experiments (Fig. 4a and 4c, 50 m⁻¹ and 120 m⁻¹, and some 100 m⁻¹ experiments). For these experiments, the absence of plucking reaching the size of the fracture spacing is likely induced by the limited extent or absence of horizontal fractures connecting the vertical network of fractures that are far apart. The low proportion of plucking for the rectangular network (10/35 mm or 120 m⁻¹) suggest that it is the largest spacing that sets the (in)efficiency of plucking, with cracks not able to develop fast enough or to develop at all to connect the fractures that are 35 mm apart. Fracture density might not be the most
885 informative variable in that case. For the smallest fracture spacing (10/10 mm or 190 m⁻¹), plucking likely dominates, as most of the blocks have dimensions very close to the fracture spacing (Fig. 4a), but it also becomes difficult to clearly separate plucking from macroabrasion at these small scales. For intermediate fracture spacing (20/20 mm and 10/20mm), both plucking and macroabrasion occur, with some experiments showing a clear dominance of plucking (Fig. 4a, 100 m⁻¹), and others a continuum between the two processes (Fig. 4a, 145 m⁻¹). Determining more precisely which of plucking and macroabrasion
890 dominates in the production of large debris is not trivial in these regimes as very large debris can result from the amalgamation of smaller events within a 2 min interval.

We conclude that the large erosion patches that we called plucking in our results are created by fracturing induced by sediment impacts exploiting the fracture network with two different subprocesses that create a continuum of block sizes: plucking resulting from the creation of horizontal fractures connecting existing ones, to create the largest blocks (Hancock et al., 1998; Whipple, 2004; Whipple et al., 2000b), and macroabrasion that create smaller debris in the vicinity of fractures (Beer and
895 Lamb, 2021; Chatanantavet and Parker, 2009, 2011). These two processes operate along classical wear abrasion by saltating bedload so that in fractured disks, a continuum between abrasion, macroabrasion and plucking exists. Yet, abrasion is systematically the dominant process, as plucking and macroabrasion never contribute more than 29 % of the total erosion compared, and have a negligible contribution, when the spacing of vertical fractures is larger than 35 mm in at least one
900 direction (Fig. 4a).

4.3 The impact of fracture geometry on erosion rates

The average erosion rate of experiments with vertical fractures does not exhibit a clear dependency on fracture density and is not significantly higher or lower than unfractured experiments (Fig. 3c), even though experiments with a higher fraction of plucking tend to have slightly higher average erosion rates (Fig. 8a) and exhibit much higher fluctuations in mean erosion rate between 2-minute intervals. We seek to explain these observations and then discuss the results obtained with dipping fractures. Many of these explanations rely on aspects of grain trajectories that we did not manage to quantify owing to the small size of the abrasion mill and the limited visibility through the scratched plexiglass and the very high turbidity.

First, unfractured experiments systematically exhibit a higher initial erosion rate close to 0.30 mm/min that subsequently decreases through time until reaching a steady value of about 0.15 mm/min after 30-40 min (Fig. 3b). Fig. 2a and 2b shows that the first 10 minutes correspond to the creation of a narrow trough in the outer part of the disk, similar to a bedrock flute in a natural channel (Hancock et al., 1998; Whipple et al., 2000b). The flute then expands inward as documented by the maps of erosion at 20 and 30 minutes (Fig. 2b). At 30-40 minutes, the flute reaches a steady width, and subsequent abrasion is at a lower rate and becomes homogeneous, except in the center of the disk which is preserved from abrasion (Fig. 8b). We postulate that the widening of the flute where active sediment transport occur, progressively reduces the number of bedload impacts per unit surface, and may slightly reduce flow velocity and/or grains saltation height as the distance to the propeller increases. The overall effect would be a reduced kinetic energy and frequency of impact per unit surface, conducive to a lower mean abrasion rate (Sklar and Dietrich, 2004).

Compared to unfractured experiments, fractured experiments exhibit key differences in the early stages: (i) there is no clear decay in mean erosion rate through time (Fig. 3a and 3b), (ii) there is no creation of a smooth flute on the outer part, although erosion tend to focus first in the outer part and then to progress inward, and (iii) the initial cumulated erosion is systematically lower than unfractured erosion for the first 20 minutes (Fig. 3a). Hence, the presence of the 3D printed fractures reduces the initial mean erosion rate. We propose two explanations for this observation: first, the softened BVOH, which sometimes sticks out by 1 or 2 mm, may dampen bedload impacts on or very close to fractures and would thus reduce the effect of abrasion. We do not believe this is a dominant component, as the initial erosion rate during the first minutes would tend to decrease with increasing fracture density and BVOH outcropping on the surface, which is not observed (Fig. 3a and b). Second, the presence of fractures quickly generates a rougher surface on the outer part of the disk due to (i) preferential abrasion or macroabrasion on or near the fractures, and/or to (ii) plucking events for high fracture densities (Fig. 2c and d). This large roughness generates additional drag that reduces flow velocity but also creates more complex flow patterns and grain trajectories after rebound. In particular, any complex rebound increasing the likelihood of grains to have an inward velocity component (directly, or after a rebound on the tank) would strongly reduce their kinetic energy due to the pronounced radial velocity gradient, compared to the smoother flute of unfractured disks that tend to keep grains within the flute. This increase in the likelihood of transversal grain trajectories is consistent with the early on occurrence of single plucking events in the center of the disk (Fig. 4a, 190 m^{-1}), and the decrease of the fraction of the surface with less than 0.5 mm of erosion as the contribution of plucking increases (Fig. 8c). For these reasons, we expect the background abrasion rate of the fractured disks to be lower than without fractures initially. This is consistent with the slightly lower average (12 %) erosion rate of experiments where plucking is negligible (Fig. 8a erosion by plucking < 5%).

Fig. 8a also shows that the average erosion slightly increases with the proportion of plucking, but only by a maximum of 20 % (0.21 mm/min for plucking > 10 % vs 0.17 mm/min for abrasion). This is explained by the limited contribution of plucking and macroabrasion to total erosion in our experiments. As explained in section 4.2, in our current setup, the rate-limiting process to generate large blocks is the rate of fracture propagation, either between existing fractures (plucking) or close to fractures (macroabrasion). This rate is likely a function of the concrete mechanical properties (including the fracture spacing itself) and the frequency and kinetic energy of impacts. These last two parameters depend on the total mass and size of the grains (Beer and Lamb, 2021) and the flow velocity that controls grain trajectories. The abrasion rate also depends on these

945 parameters (Scheingross et al., 2014; Sklar and Dietrich, 2001; Turowski et al., 2023). With our current set of parameters, the
rate of fracture propagation and its depth is not large enough compared to the efficiency of abrasion for plucking and
macroabrasion to be the dominant erosion processes. We note that plucked depth slightly increases with plucked area (scaling
exponent = 0.16) such that the smallest fracture spacing, which may generate more frequent plucking events, also creates the
shallowest ones. Intermediate fracture spacing, combining a high frequency of larger and deeper plucking events may result
950 in a higher, potentially optimal, plucking erosion rate. Fig. 4c may hint at such an optimum for a 20/20 mm spacing (145 m^{-1}).
Our exploration of the role of fracture dip for 20/20 mm spacing suggests contrasting impacts: fractures dipping at 45° results
($45/45^\circ$ or $45/67^\circ$) produce negligible plucking and limited macroabrasion (Fig. 6), behaving like lower fracture density
experiments or unfractured experiments. With vertical fractures, only 2 out of 4 experiments showed slightly higher plucking
and macroabrasion. But, one specific combination of dips ($67/90^\circ$) yielded a dramatic increase in the contribution of plucking
955 with a runaway effect, where the removal of one block led to a very rapid removal of downstream blocks in the zone where
the 67° fracture set was dipping towards the flow. The resulting pattern is particularly asymmetric, with one half of the block
largely eroded, emphasizing the critical role of the particle impact direction with the fracture dip (Fig. 6a, 157°). Because of
this asymmetry, the average erosion rate (Fig. 5c) and the contribution of plucking (Fig. 6c) tell only half of the story. If the
same level and extent of plucking had operated all over the disk, this experiment would have resulted in an average erosion
960 rate of about 0.36 mm/min , and a level of plucking of about 40 %, both much larger than all the other fractured experiments.
A repeat experiment of this specific combination of dips resulted in a similar runaway asymmetric plucking that had to be
stopped early on (supplementary material, Fig. S7). The $45/90^\circ$ combination does not exhibit such prominent plucking. We
can hypothesize that the 67° combination of fracture dip facilitates the development of horizontal fractures through shearing
followed by sliding when the block upstream face is directly exposed to grain impacts. Further experiments should explore the
965 range of dips that favor plucking and increase bedrock erosion. We conclude that amongst the fracture network characteristics
that we explored, fracture dip is the dominant control factor on erosion rates and the occurrence of plucking beyond fracture
density itself.

4.4 Comparison with previous experimental studies on plucking and abrasion

970 Previous experimental studies on bedrock incision processes have studied either abrasion (e.g., Scheingross et al., 2014; Sklar
and Dietrich, 2001; Small et al., 2015; Turowski et al., 2023), macroabrasion (Beer and Lamb, 2021), or loose block
entrainment in the context of plucking (e.g., Dubinski and Wohl, 2013; Saha et al., 2021; Wilkinson et al., 2018). Our
experimental setup with new fractured material is the first to reproduce simultaneously these 3 processes, and allow, through
detailed 3D monitoring, to follow the topographic evolution and spatio-temporal patterns of erosion rates.

975 Existing experimental studies about plucking only considered the entrainment of already loose 3D blocks (Dubinski and Wohl,
2013; Saha et al., 2021; Wilkinson et al., 2018) following the other definition of plucking used in the literature (see
introduction). These studies show that block entrainment can occur in the absence of initial bed protrusions (Wilkinson et al.,
2018), with a dynamics controlled by local hydraulic conditions (Dubinski and Wohl, 2013), and that the morphological
alterations induced by previous plucking events subsequently influence the spatial and temporal patterns of the following
980 entrainment events (Dubinski and Wohl, 2013; Wilkinson et al., 2018). These findings can be correlated with the propagation
of block removal events we observe in our experiments. Yet, while earlier studies mainly observed upstream propagation
(Dubinski and Wohl, 2013; Saha et al., 2021; Wilkinson et al., 2018), our experiments reveal plucking propagation in both
upstream and downstream directions (Fig. 4a, 6a). We hypothesize that this difference is linked to the combined effects of
sediment grain impacts and the fact that blocks are initially not detached, requiring prior fracturing to be entrained. Even if
985 these studies provide essential knowledge about how the blocks are being entrained by flow hydraulics, they did not consider
the processes that form these blocks, nor the potential role of grain impacts in the entrainment. Our experiments do not impose
block volume. Instead, depth develops naturally as the 3rd joint set or through a smaller block created by macroabrasion due

to the impacts of the saltating grains. Our analysis of the detected plucking events reveals a power-law relationship between their depth and area. We suggest that this relationship is related to the mechanical strength of the concrete we used and to the kinetic energy of the grain impacts. This added complexity fits with the importance of grains in river erosion, and with the role of fracture, which constrains the mode of erosion.

Some mill experiments using natural rocks have documented a decrease in the abrasion rate through time, followed by a stabilisation that has been interpreted as an increasing rock resistance through depth (Small et al., 2015). Other experiments did not observe such decay (Turowski et al., 2023). Here, the decay in abrasion rate is not related to a change in rock resistance, but due to the morphodynamical development of the outer flute, and particularly its initial widening. Hence, caution should be exerted when interpreting abrasion mill experiments for which a steady erosion regime has not been reached. Detailed 3D monitoring through time is essential to evaluate how significant the change in microtopography is.

4.5 Relevance to natural systems

Even if abrasion mills make important simplifications to study abrasion rates that are utterly difficult to measure in situ, they have provided key insights into the controls of rock mechanics on abrasion rates (Scheingross et al., 2014; Sklar and Dietrich, 2001; Small et al., 2015; Turowski et al., 2023). Our new fractured material is not directly designed to be an analogy of natural fractured, jointed or bedded rocks, as the fracture patterns we explored are highly simplified. But it is also this simplification and the capacity to control the mechanical discontinuities spacing and orientation that makes the problem tractable. We show that our setup can explore the simultaneous occurrence of plucking, abrasion and macroabrasion in the context of bedload transport. These processes are expected to occur in active mountain belts (Whipple et al., 2022) where bedrock rivers are never or rarely free of coarse sediment supply (e.g., Lague, 2010; Turowski et al., 2007), and where bedrock is generally full of discontinuities of various spacing and orientation due to tectonic deformation (e.g., Hartshorn et al., 2002; Molnar et al., 2007). Yet, many natural processes are not reproduced in our experimental setup, such as wedging by grains, hydraulic jacking and hydraulic pressure fluctuations within open fractures (Whipple et al., 2000b). The mechanical characteristics of our softened BVOH joints is also not fully known beyond the observation that they are much weaker than our concrete. BVOH may also damp bedload impacts and consequently reduces the efficiency of all three processes. Hence, the transfer of our results to natural systems is certainly not direct. However, insights gained through understanding the experiment morphodynamics that we carefully monitor, in relation to known boundary conditions can shed new light on process dominance in natural bedrock rivers and the role of mechanical discontinuities.

In this first set of experiments, we explored the impact of fracture patterns for a fixed sediment mass (a proxy for sediment supply in rivers), grain size, flow velocity and intact concrete strength. For these conditions, our 2D vertically fractured concrete submitted to bedload impacts erodes at a rate that does not depend strongly on the studied range of fracture density (factor 2, 0.13 ± 0.05 to 0.26 ± 0.07 mm/min) and is similar or not much larger than an unfractured concrete (~ 0.18 mm/min) (Fig. 3c). Abrasion systematically dominates all experiments, and plucking and macroabrasion are either negligible for large fracture spacing (above 35 mm), or contributing a maximum of 29 % of the total erosion for smaller fracture spacing (10 to 20 mm). We interpret this as resulting from the impact-driven rate of fracture propagation between pre-existing fracture being too slow, compared to the abrasion rates, for plucking to be dominant. A different choice of concrete strength, grain sizes, sediment mass, and flow velocity could lead to a different balance between these two competing processes. Further experiments are thus needed to expand the parameter space of the erosion efficiency problem in our experimental setup.

Nonetheless, these results show that a rock with a high density of 2D mechanical discontinuities that are not fully connected in 3D does not necessarily erode much faster than the same intact rock when bedload transport and abrasion occur. This is consistent with the view put forward by various authors, that the rate of crack propagation between pre-existing fractures is a critical parameter for plucking to be a dominant process in nature (Chatanantavet and Parker, 2009; Hancock et al., 1998; Scott and Wohl, 2019; Whipple et al., 2000b). Our experiments also show that even though plucking can occur all over the surface

1030 leaving a clear morphological signature (Fig. 2e and 4a, 145 m-1), it does not imply that plucking is the dominant erosion
process. Another key insight is that very different bedrock morphologies in relation to the presence or absence of fractures
(Fig. 2a and 2e) can result in very similar time averaged erosion rates. Lastly, our experiments demonstrate that the fracture
dip and orientation in relation to flow and impacts direction was a dominant controlling factor (from 0.13 mm/min to 0.36
mm/min when corrected for asymmetry) compared to the effect of fracture spacing for vertical configurations (0.13 mm/min
to 0.26 mm/min). This is consistent with observations in natural rivers (Scott and Wohl, 2019; Wohl, 2000). Our experiments
1035 suggest that plucking efficiency has a non-linear dependency with the dip angle (Fig. 6c) that should be further explored.

5 Conclusions

In this study, we developed a new artificial bedrock made of concrete with 3D printed fracture patterns acting as planar
discontinuities that we use in a classical “abrasion mill” experimental setup (Sklar and Dietrich, 2001). We investigate how
the spacing and dip of regular fracture can affect the magnitude, the location, and the mode of erosion, between two classes of
1040 processes: abrasion and plucking. We also explore if macroabrasion creating smaller debris than fracture spacing occurs in our
experiment. We use high-frequency temporal series of 3D topographies to document erosion rates and patterns through time.
We show that in the absence of fractures, the disks erode by wear abrasion only, without macroabrasion, and exhibit a
progressive decay of the average erosion rate due to the vertical incision and inward widening of a flute-like feature near the
mill edge. Erosion rate then become steady at about half the initial erosion rate. The resulting topography is smooth with radial
1045 symmetry. When the disk is fractured, erosion can occur both by abrasion, macroabrasion and plucking, a unique feature of
our artificial bedrock and key contribution of this study. Macroabrasion occurs near fractures and dominates plucking for high
fracture spacing, while plucking tend to dominate macroabrasion for low fracture densities, even though it is difficult to
precisely quantify the relative importance of both. The erosion rate of fractured experiments does not show a temporal decay
but exhibits sharp variations over 2-min intervals due to plucking events. The resulting topographies are rougher with less
1050 radial symmetry. Plucking can occur closer to the disk center compared to abraded unfractured disks, hinting at more complex
grain trajectories owing to the larger roughness. Even though plucking can occur over most of the surface in the intermediate
to highest fracture densities, abrasion always dominates plucking and macroabrasion in terms of total erosion budget for all
studied fracture spacing and geometries. We posit that the rate of horizontal fracture propagation driven by bedload impacts is
too slow and the pluckable depth to shallow for plucking to dominate abrasion. This also explain why erosion rates show little
1055 increase with fracture density (factor 2 at most). Further experiments are needed to determine whether the abrasion dominance
observed in our experiments is a result of our specific choice of sediment mass, grain size, flow velocity, and mechanical
properties of the concrete and the 3D printing material (BVOH). Finally, we demonstrate that in our experiments the orientation
and dip of the fractures with respect to the flow plays a dominant role compared to fracture density, in enhancing plucking.
Plucking is favoured when fractures dip upstream (i.e., against the flow direction) and only for one specific dip angle (67°)
1060 amongst the 3 studied (45° and 90°).

Our results emphasize the critical role that the creation of 3rd fracture both in term of depth and propagation rate has for
plucking to dominate abrasion in areas where only 2 set of mechanical discontinuities exists (Chatanantavet and Parker, 2009,
2011; Scott and Wohl, 2019; Whipple et al., 2000b). Compared to our experiments, a larger range of processes can contribute
to this 3rd fracture in natural systems including wedging by grains (Hartshorn et al., 2002), wetting and drying, temperature
1065 fluctuations (Whipple et al., 2022). Additional complexities related to discharge fluctuations, sediment supply fluctuations and
the large range of grain size and fracture spacing can also alter the efficiency of abrasion and plucking. It is thus difficult to
evaluate how specific to natural systems is the balance between abrasion and plucking that we obtain in our experiments.
However, we demonstrate that the classical view that densely jointed rock erodes much faster than the same intact rock (Molnar

et al., 2007; Thuro, 1997) is not always true. We also illustrate how very different bedrock morphologies, typical of abrasion and plucking processes of the same rock material intact or fractured, can have very similar time-averaged erosion rates.

<u>n</u>	<u>Spacing (mm)</u>	<u>Density (m⁻¹)</u>	<u>Dip angle (°)</u>	<u>Sum of dip angle (°)</u>	<u>Mean erosion rate (mm/min)</u>	<u>Standard deviation (mm/min)</u>	<u>Erosion by plucking (%)</u>
<u>1</u>	<u>=</u>	<u>0</u>	<u>=</u>	<u>=</u>	<u>0.18</u>	<u>0.05</u>	<u>0</u>
<u>2</u>					<u>0.19</u>	<u>0.06</u>	<u>0</u>
<u>3</u>					<u>0.16</u>	<u>0.04</u>	<u>0</u>
<u>4</u>					<u>0.17</u>	<u>0.05</u>	<u>0</u>
<u>5</u>	<u>40/40</u>	<u>50</u>	<u>90/90</u>	<u>180</u>	<u>0.16</u>	<u>0.04</u>	<u>1</u>
<u>6</u>					<u>0.14</u>	<u>0.03</u>	<u>1</u>
<u>7</u>	<u>20/20</u>	<u>100</u>	<u>90/90</u>	<u>180</u>	<u>0.24</u>	<u>0.03</u>	<u>8</u>
<u>8</u>					<u>0.21</u>	<u>0.02</u>	<u>1</u>
<u>9</u>					<u>0.17</u>	<u>0.04</u>	<u>7</u>
<u>10</u>					<u>0.13</u>	<u>0.03</u>	<u>2</u>
<u>11</u>			<u>45/45</u>	<u>90</u>	<u>0.14</u>	<u>0.03</u>	<u>1</u>
<u>12</u>					<u>0.14</u>	<u>0.03</u>	<u>1</u>
<u>13</u>			<u>45/67</u>	<u>112</u>	<u>0.14</u>	<u>0.03</u>	<u>1</u>
<u>14</u>			<u>67/67</u>	<u>134</u>	<u>0.16</u>	<u>0.06</u>	<u>6</u>
<u>15</u>					<u>0.14</u>	<u>0.05</u>	<u>8</u>
<u>16</u>					<u>0.13</u>	<u>0.04</u>	<u>9</u>
<u>17</u>			<u>90/45</u>	<u>135</u>	<u>0.22</u>	<u>0.04</u>	<u>9</u>
<u>18</u>			<u>90/67</u>	<u>157</u>	<u>0.19</u>	<u>0.05</u>	<u>22</u>
<u>19</u>	<u>10/35</u>	<u>120</u>	<u>90/90</u>	<u>180</u>	<u>0.13</u>	<u>0.05</u>	<u>1</u>
<u>20</u>	<u>10/20</u>	<u>145</u>	<u>90/90</u>	<u>180</u>	<u>0.17</u>	<u>0.05</u>	<u>9</u>
<u>21</u>					<u>0.26</u>	<u>0.07</u>	<u>29</u>
<u>22</u>	<u>10/10</u>	<u>190</u>	<u>90/90</u>	<u>180</u>	<u>0.20</u>	<u>0.08</u>	<u>9</u>
<u>23</u>					<u>0.17</u>	<u>0.04</u>	<u>19</u>

Table 1: Geometric properties, mean erosion rates with standard deviations and percentage of erosion by plucking for all the experiments. The colours to the right of density and sum of dip angle are the ones used in the figures.

Data availability.

Data generated in this study are available online in the Zenodo repository (<https://doi.org/10.5281/zenodo.17607654>).

Authors contributions.

1075 MF and LG conducted the experiments. JJK assisted in the experimental setup and 3D printing of fracture networks. CL enabled us to perform the strength tests on our concrete. PL initiated the development of a Python code to automate calculations on our point clouds. MF, LG and PS performed the analysis and prepared the figures. HH helped us for the plucking detection. CA initiated the development of the experimental setup. MF, LG, PS, and DL contributed to the writing and revision of the manuscript.

Competing interests.

1080 The authors declare that they have no conflict of interest.

Acknowledgements.

The authors would like to thank the two anonymous referees and Dr. Neely, who provided valuable comments that helped to improve and clarify the article. Finally, we thank the handling associate editor, Anastasia Piliouras, for her constructive feedback and suggestions.

Financial support.

This research has been supported by the European Research Council, H2020 European Research Council (FEASIBLE (grant no. 803721)). We also acknowledge support by the University of Rennes and the French Ministry of Scientific Research.

References

[s.n.]: Le durcissement du béton, *Bulletin du Ciment*, Service de Recherches et Conseils Techniques de l'Industrie Suisse du Ciment (TFB AG), 18–19, 13, <https://doi.org/10.5169/seals-145354>, 1950–1951.

AFNOR: NF EN 196-1: Methods of testing cement - Part 1: determination of strength, AFNOR Éditions, <https://www.boutique.afnor.org/en-gb/standard/nf-en-1961/methods-of-testing-cement-part-1-determination-of-strength/fa184622/57803>, 2016.

Anderson, R. S. and Anderson, S. P.: Geomorphology: ~~the mechanics~~The Mechanics and ~~chemistry~~Chemistry of ~~landscapes~~Landscapes, Cambridge University Press, ISBN 10 0521519780, 2010.

Attal, M., Lavé, J., and Masson, J.-P.: New Facility to Study River Abrasion Processes, *Journal of Hydraulic Engineering, J. Hydraul. Eng.*, 132, 624–628, [https://doi.org/10.1061/\(ASCE\)0733-9429\(2006\)132:6\(624\)](https://doi.org/10.1061/(ASCE)0733-9429(2006)132:6(624)), 2006.

Beer, A. R. and Lamb, M. P.: Abrasion regimes in fluvial bedrock incision, *Geology*, 49, 682–386, <https://doi.org/10.1130/G48466.1>, 2021.

Beer, A. R. and Turowski, J. M.: Bedload transport controls bedrock erosion under sediment-starved conditions, *Earth Surface Dynamics*, 3, 291–309, <https://doi.org/10.5194/esurf-3-291-2015>, 2015.

Beer, Alexander R., Turowski, J. M., and Kirchner, J. W.: Spatial patterns of erosion in a bedrock gorge, *Journal of Geophysical Research: J. Geophys. Res. Earth Surface, Surf.*, 122, 191–214, <https://doi.org/10.1002/2016JF003850>, 2017.

Bonnet, E., Bour, O., Odling, N. E., Davy, P., Main, I., Cowie, P., and Berkowitz, B.: Scaling of fracture systems in geological media, *Reviews of Geophysics, Rev. Geophys.*, 39, 347–383, <https://doi.org/10.1029/1999RG000074>, 2001.

Brodu, N. and Lague, D.: 3D terrestrial lidar data classification of complex natural scenes using a multi-scale dimensionality criterion: Applications in geomorphology, *ISPRS Journal of Photogrammetry and Remote Sensing*, 68, 121–134, <https://doi.org/10.1016/j.isprsjprs.2012.01.006>, 2012.

Bursztyn, N., Pederson, J. L., Tressler, C., Mackley, R. D., and Mitchell, K. J.: Rock strength along a fluvial transect of the Colorado Plateau—quantifying a fundamental control on geomorphology, *Earth and Planetary Science Letters*, 429, 90–100, <https://doi.org/10.1016/j.epsl.2015.07.042>, 2015.

Carr, J. C., DiBiase, R. A., Yeh, E. C., Fisher, D. M., and Kirby, E.: Rock properties and sediment caliber govern bedrock river morphology across the Taiwan Central Range, *Science Advances*, 9, eadg6794, <https://doi.org/10.1126/sciadv.adg6794>, 2023.

Chatanantavet, P. and Parker, G.: Experimental study of bedrock channel alluviation under varied sediment supply and hydraulic conditions, *Water Resources Research*, 44, <https://doi.org/10.1029/2007WR006581>, 2008.

Chatanantavet, P. and Parker, G.: Physically based modeling of bedrock incision by abrasion, plucking, and macroabrasion, *Journal of Geophysical Research: Earth Surface, J. Geophys. Res.*, 114, <https://doi.org/10.1029/2008JF001044>, 2009.

- 1120 ~~Colaianne, N. J., Shobe, C. M., Moler, J., Benison, K. C., and Chilton, K. D.: Beyond boundaries: Depositional environment controls on erodibility, process, and form in rivers incising sedimentary bedrock, *Geosphere*, <https://doi.org/10.1130/GES02791.1>, 2024.~~
- ~~[Chatanantavet, P. and Parker, G.: Quantitative Testing of Model of Bedrock Channel Incision by Plucking and Macroabrasion, *J. Hydraul. Eng.*, 137, 1311–1317, \[https://doi.org/10.1061/\\(ASCE\\)HY.1943-7900.0000421\]\(https://doi.org/10.1061/\(ASCE\)HY.1943-7900.0000421\), 2011.](#)~~
- 1125 Dershowitz, W. S. and Herda, H. H.: Interpretation of fracture spacing and intensity, *in: The 33rd U.S. Symposium on Rock Mechanics (USRMS)*, edited by: Tillerson & Wawersik, 1992 Balkema, Rotterdam, ISBN 90 5410 045, 1992.
- DiBiase, R. A., Rossi, M. W., and Neely, A. B.: Fracture density and grain size controls on the relief structure of bedrock landscapes, *Geology*, 46, 399–402, <https://doi.org/10.1130/G40006.1>, 2018.
- 1130 Dubinski, I. M. and Wohl, E.: Relationships between block quarrying, bed shear stress, and stream power: A physical model of block quarrying of a jointed bedrock channel, *Geomorphology*, 180–181, 66–81, <https://doi.org/10.1016/j.geomorph.2012.09.007>, 2013.
- Ehlen, J. and Wohl, E.: Joints and landform evolution in bedrock canyons, ~~*Transactions, Japanese Geomorphological Trans. Jpn. Geomorphol.*~~ Union, 23, 237–255, 2002.
- 1135 Eppes, M. C., Rinehart, A., Aldred, J., Berberich, S., Dahlquist, M. P., Evans, S. G., Keanini, R., Laubach, S. E., Moser, F., Morovati, M., Porson, S., Rasmussen, M., and Shaanan, U.: Introducing standardized field methods for fracture-focused surface process research, *Earth Surface Dynamics, Surf. Dynam.*, 12, 35–66, <https://doi.org/10.5194/esurf-12-35-2024>, 2024.
- ~~Féret, R.: Sur la compacité des mortiers hydrauliques, *Annales des Ponts et Chaussées, Mémoires et Documents relatifs à l'art des constructions et au service de l'ingénieur*, 4, 5–164, 1892.~~
- 1140 ~~Forte, A. M., YanitesHallet, B.-J.: Glacial quarrying: a simple theoretical model, *Annals of Glaciology*, 22, 1–8, <https://doi.org/10.3189/1996AoG22-1-1-8>, 1996.~~
- ~~Hancock, G. S., Anderson, R. S., and Whipple, K. X.: Complexities of landscape evolution during Beyond power: Bedrock river incision through layered stratigraphy with contrasts process and form, *in: rock strength, Earth Surface: Rivers Over Rock: Fluvial Processes in Bedrock Channels*, vol. 107, edited by: Tinkler, K. J. and Landforms, 41, 1736–1757 Wohl, E. E., Blackwell Publishing Ltd, 35–60, <https://doi.org/10.1002/esp.3947>, 20161029/GM107p0035, 1998.~~
- 1145 ~~Grant, A., Regez, B., Kocak, S., Huber, J. D., and Mooers, A.: Anisotropic properties of 3-D printed Poly Lactic Acid (PLA) and Acrylonitrile Butadiene Styrene (ABS) plastics, *Results in Materials*, 12, 100227, <https://doi.org/10.1016/j.rinma.2021.100227>, 2021.~~
- ~~Hartshorn, K., Hovius, N., Dade, W. B., and Slingerland, R. L.: Climate-Driven Bedrock Incision in an Active Mountain Belt, *Science*, 297, 2036–2038, <https://doi.org/10.1126/science.1075078>, 2002.~~
- 1150 Hurst, A. A., Anderson, R. S., and Crimaldi, J. P.: Toward Entrainment Thresholds in Fluvial Plucking, *Journal of Geophysical Research: Earth Surface*, 126, e2020JF005944, <https://doi.org/10.1029/2020JF005944>, 2021.
- ~~Jansen, J. D., Codilean, A. T., Bishop, P., and Hoey, T. B.: Scale Dependence of Lithological Control on Topography: Bedrock Channel Geometry and Catchment Morphometry in Western Scotland, *The Journal of Geology*, 18, 223–246, <https://doi.org/10.1086/651273>, 2010.~~
- 1155 Lague, D.: Reduction of long-term bedrock incision efficiency by short-term alluvial cover intermittency, *Journal of Geophysical Research: Earth Surface*, 115, <https://doi.org/10.1029/2008JF001210>, 2010.
- ~~Lague, D.: The stream power river incision model: evidence, theory and beyond, *Earth Surface Processes and Landforms*, 39, 38–61, <https://doi.org/10.1002/esp.3462>, 2014.~~
- 1160 ~~Lague, D., Brodu, N., and Leroux, J.: Accurate 3D comparison of complex topography with terrestrial laser scanner: Application to the Rangitikei canyon (N-Z), *ISPRS Journal of Photogrammetry and Remote Sensing*, 82, 10–26, <https://doi.org/10.1016/j.isprsjprs.2013.04.009>, 2013.~~
- ~~Lamb, M. P. and Dietrich, W. E.: The persistence of waterfalls in fractured rock, *GSA Bulletin*, 121, 1123–1134, <https://doi.org/10.1130/B26482.1>, 2009.~~

- 165 Le Goc, R., Pinier, B., Darcel, C., Lavoine, E., Doolaege, D., de Simone, S., De Dreuzy, J.-R., and Davy, P.: DFN. lab: software platform for Discrete Fracture Network models, AGU Fall Meeting 2019, [San Francisco CA, 9-13 December 2019, H41H-1778, 2019-2019.](#)
- Lima, A. G., Pelegrina, M. A., Pontarolo, M., Gonçalves Lima, A., Pelegrina, M. A., and Pontarolo, M.: Fracture variability in basalts and its effect on river erosion: a case study in the Paraná volcanic province, *Earth Sciences Research Journal, Sci. Res. J.*, 25, 13–19, <https://doi.org/10.15446/esrj.v25n1.85098>, 2021.
- 170 Molnar, P., Anderson, R. S., and Anderson, S. P.: Tectonics, fracturing of rock, and erosion, *Journal of Geophysical Research: Earth Surface, J. Geophys. Res.*, 112, <https://doi.org/10.1029/2005JF000433>, 2007.
- ~~Neely, A. B. and DiBiase, R. A.: Drainage Area, Bedrock Fracture Spacing, and Weathering Controls on Landscape Scale Patterns in Surface Sediment Grain Size, *Journal of Geophysical Research: Earth Surface*, 125, e2020JF005560, <https://doi.org/10.1029/2020JF005560>, 2020.~~
- 175 Neely, A. B., DiBiase, R. A., Corbett, L. B., Bierman, P. R., and Caffee, M. W.: Bedrock fracture density controls on hillslope erodibility in steep, rocky landscapes with patchy soil cover, southern California, USA, *Earth and Planetary Science Letters, Planet. Sci. Lett.*, 522, 186–197, <https://doi.org/10.1016/j.epsl.2019.06.011>, 2019.
- Paola, C., Straub, K., Mohrig, D., and Reinhardt, L.: The “unreasonable effectiveness” of stratigraphic and geomorphic experiments, *Earth Science Reviews, Sci. Rev.*, 97, 1–43, <https://doi.org/10.1016/j.earscirev.2009.05.003>, 2009.
- 180 ~~Pettifer, G. S. and Fookes, P. G.: A revision of the graphical method for assessing the excavatability of rock, *Quarterly Journal of Engineering Geology and Hydrogeology*, 27, 145–164, <https://doi.org/10.1144/GSL.QJEGH.1994.027.P2.05>, 1994.~~
- Saha, R., Lee, J. S., and Hong, S. H.: The impact of lateral flow contraction on the rock plucking process under sub-critical flow conditions, *Earth Surface Processes and Surf. Process. Landforms*, 46, 2902–2915, <https://doi.org/10.1002/esp.5220>, 2021.
- 185 ~~Scheingross, J., Brun, F., Lo, D., Omerdin, K., and Lamb, M.: Experimental evidence for fluvial bedrock incision by suspended and bedload sediment, *Geology*, 42, 523–526, <https://doi.org/10.1130/G35432.1>, 2014.~~
- Scott, D. N. and Wohl, E. E.: Bedrock fracture influences on geomorphic process and form across process domains and scales, *Earth Surface Processes and Surf. Process. Landforms*, 44, 27–45, <https://doi.org/10.1002/esp.4473>, 2018-2019.
- 190 Sklar, L. and Dietrich, W.: Sediment and rock strength control on river incision into bedrock, *Geology*, 29, 1087–1090, [https://doi.org/10.1130/0091-7613\(2001\)029<1087:SARSCO>2.0.CO;2](https://doi.org/10.1130/0091-7613(2001)029<1087:SARSCO>2.0.CO;2), 2001.
- ~~Sklar, L. and Dietrich, W. E.: River Longitudinal Profiles and Bedrock Incision Models: Stream Power and the Influence of Sediment Supply, in: Rivers Over Rock: Fluvial Processes in Bedrock Channels, vol. 107, American Geophysical Union (AGU), 237–260, <https://doi.org/10.1029/GM107p0237>, 1998.~~
- 195 ~~Sklar, L. S. and Dietrich, W. E.: A mechanistic model for river incision into bedrock by saltating bed load, *Water Resour. Res.*, 40, <https://doi.org/10.1029/2003WR002496>, 2004.~~
- ~~Small, E. E., Blom, T., Hancock, G. S., Hynek, B. M., and Wobus, C. W.: Variability of rock erodibility in bedrock-floored stream channels based on abrasion mill experiments, *J. Geophys. Res. Earth Surf.*, 120, 1455–1469, <https://doi.org/10.1002/2015JF003506>, 2015.~~
- 200 ~~Snyder, N. P., Whipple, K. X., Tucker, G. E., and Merritts, D. J.: Channel response to tectonic forcing: field analysis Importance of stream morphology a stochastic distribution of floods and hydrology erosion thresholds in the Mendocino triple junction region, northern California, *Geomorphology*, 53, 97–127 bedrock river incision problem, *J. Geophys. Res. Solid Earth*, 108, [https://doi.org/10.1016/S0169-555X\(02\)00349-5](https://doi.org/10.1016/S0169-555X(02)00349-5) 1029/2001JB001655, 2003.~~
- Thuro, K.: Drillability prediction: geological influences in hard rock drill and blast tunnelling, *Geologische Rundschau, Geol. Rundsch.*, 86, 426–438, <https://doi.org/10.1007/s005310050151>, 1997.
- 205 ~~Turowski, J. M., Pruß, G., Lague, D., and Reich, M.: Experimental Design Hovius, N.: Cover effect in bedrock abrasion: A new derivation and Protocol its implications for Standardized Measurements the modeling of Rock Erodibility in Fluvial Impact Erosion, *Journal of Hydraulic Engineering*, 149, 06023010 bedrock channel morphology, *J. Geophys. Res. Earth Surf.*, 112, <https://doi.org/10.1061/JHEND8.HYENG-13346>, 2023a 1029/2006JF000697, 2007.~~

- 1210 Turowski, J. M., Pruß, G., Voigtländer, A., Ludwig, A., Landgraf, A., Kober, F., and Bonnelye, A.: Geotechnical controls on erodibility in fluvial impact erosion, *Earth Surface Dynamics, Surf. Dynam.*, 11, 979–994, <https://doi.org/10.5194/esurf-11-979-2023>, 2023b2023.
- ~~Vervoort, A. and De Wit, K.: Correlation between dredgeability and mechanical properties of rock, *Engineering Geology*, 47, 259–267, [https://doi.org/10.1016/S0013-7952\(97\)00023-9](https://doi.org/10.1016/S0013-7952(97)00023-9), 1997.~~
- 1215 Whipple, K. X.: Bedrock Rivers and the Geomorphology of Active Orogens, *Annual Review of Annu. Rev. Earth and Planetary Sciences, Planet. Sci.*, 32, 151–185, <https://doi.org/10.1146/annurev.earth.32.101802.120356>, 2004.
- ~~Whipple, K. X. and Tucker, G. E.: Dynamics of the stream power river incision model: Implications for height limits of mountain ranges, landscape response timescales, and research needs, *Journal of Geophysical Research*, 104, 17661–17674, <https://doi.org/10.1029/1999JB900120>, 1999.~~
- 1220 Whipple, K. X., Snyder, N. P., and Dollenmayer, K.: Rates and processes of bedrock incision by the Upper Ukak River since the 1912 Novarupta ash flow in the Valley of Ten Thousand Smokes, Alaska, *Geology*, 28, 835–838, [https://doi.org/10.1130/0091-7613\(2000\)28<835:RAPOBI>2.0.CO;2](https://doi.org/10.1130/0091-7613(2000)28<835:RAPOBI>2.0.CO;2), 2000a.
- Whipple, K. X., Hancock, G. S., and Anderson, R.: River incision into bedrock: Mechanics and relative efficacy of plucking, abrasion, and cavitation, *Geological Society of America GSA Bulletin*, 112, 490–503, [https://doi.org/10.1130/0016-7606\(2000\)112<490:RIIBMA>2.0.CO;2](https://doi.org/10.1130/0016-7606(2000)112<490:RIIBMA>2.0.CO;2), 2000b.
- 1225 Whipple, K. X., DiBiase, R. A., Crosby, B., and Johnson, J. P. L.: 6.40 Bedrock Rivers, in: *Treatise on Geomorphology (Second Edition)*, edited by: Shroder, J. (Jack) F., Academic Press, Oxford, 865–903, <https://doi.org/10.1016/B978-0-12-818234-5.00101-2>, 2022.
- Wilkinson, C., Harbor, D. J., Helgans, E., and Kuehner, J. P.: Plucking phenomena in nonuniform flow, *Geosphere*, 14, 2157–2170, <https://doi.org/10.1130/GES01623.1>, 2018.
- 1230 ~~Wilson, A. and Lavé, J.: Convergent evolution of abrading flow obstacles: Insights from analogue modelling of fluvial bedrock abrasion by coarse bedload, *Geomorphology*, 208, 207–224, <https://doi.org/10.1016/j.geomorph.2013.11.024>, 2014.~~
- Wohl, E.: The effect of bedrock jointing on the formation of straths in the Cache la Poudre River drainage, Colorado Front Range, *Journal of Geophysical Research: J. Geophys. Res. Earth Surface, Surf.*, 113, F01007, <https://doi.org/10.1029/2007JF000817>, 2008.
- 1235 ~~Wohl, E. E.: Substrate Influences on Step-Pool Sequences in the Christopher Creek Drainage, Arizona, *J Geol*, 108, 121–129, <https://doi.org/10.1086/314385>, 2000.~~
- Yanites, B. J.: The Dynamics of Channel Slope, Width, and Sediment in Actively Eroding Bedrock River Systems, *Journal of Geophysical Research: J. Geophys. Res. Earth Surface, Surf.*, 123, 1504–1527, <https://doi.org/10.1029/2017JF004405>, 2018.
- ~~Zondervan, J. R., Whittaker, A. C., Bell, R. E., Watkins, S. E., Brooke, S. A. S., and Hann, M. G.: New constraints on bedrock erodibility and landscape response times upstream of an active fault, *Geomorphology*, 351, 106937, <https://doi.org/10.1016/j.geomorph.2019.106937>, 2020.~~